An Accurate and Universal Method for the Anharmonic Vibrational Analysis of the Raman Active C≡C Stretch of Terminal Alkynes

Authors:

Kristina Streu[1], Sara Hunsberger[1], Jeanette Patel[1], Xiang Wan[2], and Clyde A. Daly Jr. [1],*

[1] Department of Chemistry, Haverford College, Haverford PA 19041
[2] Department of Mathematics and Statistics, Loyola University Chicago, Chicago, IL, 60660
*Corresponding author, cdaly2@haverford.edu

Abstract

The terminal alkyne C≡C stretch has a large Raman scattering cross section in the "silent" region for biomolecules. This has led to many Raman tag and probe studies using this moiety to study biomolecular systems. Computational investigation of these systems is vital to aid in the interpretation of the results. In this work, we develop a method for computing terminal alkyne vibrational frequencies and transition isotropic polarizabilities which can easily and accurately be applied to any terminal alkyne molecule. Our tool applies the discrete variable representation method to a localized version of the C≡C stretch normal mode. The errors of (1) localization to the terminal alkyne moiety, (2) anharmonic normal mode isolation inherent in the single-dimensional discrete variable representation method, and (3) discretization of the Born-Oppenheimer potential energy surface are quantified and found to be generally small and cancel each other. This results in a method with low error compared to other anharmonic vibrational methods like VPT2 and to experiment. Several density functionals are tested using the method, and TPSS-D3 is found to perform surprisingly well. Diffuse basis functions are found to be important for the accuracy of computed frequencies. Finally, the computation of vibrational properties like transition isotropic polarizabilities and dipole moments and the universality of the normal mode atomic displacements across molecules are demonstrated.

I. Introduction

Infrared and Raman spectroscopy are invaluable tools for investigating the structure and dynamics of chemically complex systems such as biomolecules, liquids, solutions, molecular clusters, the atmosphere, and others.[1–10] When possible, effective vibrational probes can be used to investigate specific aspects of these systems.[1] For instance, OH, OD, and cyanide moieties are effective probes of the hydrogen bonding potential of an environment and carbonyls and nitriles have been used as probes of the electric fields of an environment.[11–22] An optimal vibrational probe is non-perturbative to the system and an investigation of the probe directly investigates the system property of interest. Recent work on the solvation of CO_2 in ionic liquids exemplifies this; here, the CO_2 was the probe of its own solvation dynamics.[23–25]

The triple bond CC stretch of alkynes has long been used as a Raman tag in biomolecular and surface enhanced Raman spectroscopy studies.[26–32] This vibration appears in the biomolecular "Raman window," a portion of the spectrum where biomolecular systems rarely produce Raman scattering.[9,33–35] In the prior tagging studies, the alkyne vibration was used mainly to show the presence of a material it was attached to. However, recent work has turned to exploring the terminal alkyne CC stretch as a possible vibrational solvatochromic probe.[36–42] In a solvatochromic probe study, details of the lineshape, frequency, and intensity of the absorption are used to infer the alkyne probe's molecular environment.

We follow recent work at Haverford College and elsewhere showing that the terminal alkyne CC stretch vibrational mode is (1) an effective probe of biomolecular structure and dynamics and (2) independently sensitive to both its solvent and substituent.[36,38,39] A third question remains unanswered: *what, specifically, is the alkyne probe reporting on?* There are several possibilities given the available experimental data. The work of Epstein et al. and Dong et al. implies that the terminal alkyne detects the hydrophilicity or hydrogen bonding potential of the environment.[39,42] However, Romei et al. complicate this picture; they find that the terminal alkyne vibration is sensitive to a number of solvents with different properties.[38] They correlate this sensitivity with empirical scales of the propensity of the solvent to donate electrons or polarize. Even so, it is possible that the factors which cause a probe's frequency to shift *between solvents* are distinct from those that cause the frequency to shift *between configurations* in a single solvent, complicating the question of reporting. There are also possible effects arising from covalently bonded substituents; some experiments have shown that electronic conjugation of the alkyne triple bond or adding sulfur or silicon atoms can shift the scatting frequency, change the scattering intensity, or modify the population lifetime.[31,36,38,42–47]

In this paper, we take our first steps towards a full quantum chemistry and molecular dynamics investigation of what the alkyne vibration is specifically reporting on. Here, we develop a new method for calculating the frequency of a terminal alkyne which is compatible with snapshots extracted from molecular dynamics simulations. Our goals are to:

1. Demonstrate that an isolated and localized discrete variable representation method is sufficient to compute the terminal alkyne CC-stretch normal mode vibrational frequency with good accuracy.
2. Select one or more density functional theory methods which show good accuracy and speed for further examination in the presence of solvent in future work.

3. Propose a universal set of terminal alkyne CC stretch normal mode atom displacements, and show that the computed vibrational properties have the expected features.

Our final method *localizes, isolates,* and *discretizes* the terminal alkyne CC-stretch vibrational normal mode. We quantify the errors associated with each of these assumptions; discretization is fairly benign, but localization and isolation errors are larger. Fortunately, these errors are themselves moderate and each shift the alkyne frequency in the opposite direction, nearly canceling out. We also attempt to lay out a particularly clear theoretical description of our employed discrete variable method in Section II.

Here, alkynes are dealt with in the gas phase, providing a solid foundation for future work in condensed phase with substantial non-covalent interactions. This also allows us to examine the effect of substituent on the alkyne frequency and other vibrational properties. We examine eight terminal alkyne molecules (Figure 2). Six are particularly small, having four or fewer atoms heavier than hydrogen. These molecules can be examined using highly accurate electronic (CCSD(T) and MP2) and vibrational (TOSH and VPT2) structure methods. These molecules will be used in the first section of our results to quantify errors associated with localization, isolation, and discretization. The remaining molecules are used to quantify substituent effects and explore the accuracy of a set of models of the electronic structure based on DFT.

II. Theory

An anharmonically isolated normal mode can be treated as quantum particle in a single dimension with the Hamiltonian

$$\hat{H} = \frac{\hat{p}_Q^2}{2\mu_Q} + \hat{V}(Q) \tag{1}$$

where $\hat{V}(Q)$ is the potential energy operator as a function of the normal mode coordinate Q and $\hat{p}_Q$ is the momentum operator conjugate to that coordinate.[48] The normal mode coordinate can be written as a sum over atomic displacements away from the optimized geometry

$$Q = \sum_{j=1}^{3N} \frac{\partial Q}{\partial c_j} \left(c_j - c_{j,0} \right) \tag{2}$$

where N is the number of atoms (so $3N$ is the number of cartesian coordinates), c_j is the j th atomic cartesian coordinate, and $c_{j,0}$ is the j th optimized atomic cartesian coordinate.[48] If all the $c_j = c_{j,0}$, the molecular geometry is optimized, the energy is at a minimum, and $Q = 0$. A normal mode vibration changes the molecular geometry according to the derivatives $\frac{\partial Q}{\partial c_j}$. The inverses of these derivatives, $\frac{\partial c_j}{\partial Q}$, are printed out by most quantum chemistry programs following a harmonic frequency calculation and are often called "normal mode atomic displacements."[48] The reduced mass for a normal mode is given by

$$\mu_Q = \frac{\sum_{j=1}^{3N} \left(\sqrt{m_j} \frac{\partial c_j}{\partial Q} \right)^2}{\sum_{j=1}^{3N} \left(\frac{\partial c_j}{\partial Q} \right)^2} \tag{3}$$

where m_j is the mass of the atom with cartesian coordinate c_j and the other symbols retain their meaning.[49] In the harmonic oscillator approximation, the potential energy of the vibrational Hamiltonian is expanded in a Taylor series about the minimum energy position. By definition, the normal mode coordinate has a value of zero at the minimum energy position. This gives

$$\hat{H} = \frac{\hat{p}_Q^2}{2\mu_Q} + \sum_{n=0}^{\infty} \left(\frac{\partial^n V(Q)}{\partial Q^n} \right)_{Q=0} \frac{\hat{Q}^n}{n!} \tag{4}$$

The $n = 0$ term (the energy of the optimized geometry) can be arbitrarily set to zero. If $Q \approx 0$, then the first order term is nearly zero because the first derivative at a stationary point is zero. The higher order terms will also be small since (1) $Q \approx 0$ and is being raised to increasing exponents and (2) the dividing factorial terms increase as the order of the expansion increases. The most slowly shrinking term of the potential as $Q \to 0$ is the second order term, so we get

$$\hat{H} = \frac{\hat{p}_Q^2}{2\mu_Q} + \frac{1}{2} \left(\frac{\partial^2 V(Q)}{\partial Q^2} \right)_{Q=0} \hat{Q}^2 \tag{5}$$

which is the harmonic oscillator Hamiltonian for which the solutions are well known.[48;50] The most popular techniques for including anharmonicity are based on including the third and fourth order terms in the Hamiltonian, but still require the first derivative of the energy to be nearly zero,

$$\hat{H} = \frac{\hat{p}_Q^2}{2\mu_Q} + \frac{1}{2} \left(\frac{\partial^2 V(Q)}{\partial Q^2} \right)_{Q=0} \hat{Q}^2 + \frac{1}{6} \left(\frac{\partial^3 V(Q)}{\partial Q^3} \right)_{Q=0} \hat{Q}^3 + \frac{1}{24} \left(\frac{\partial^4 V(Q)}{\partial Q^4} \right)_{Q=0} \hat{Q}^4 \tag{6}$$

The vibrational configuration interaction (VCI), second-order vibrational perturbation theory (VPT2), vibrational self-consistent field (VSCF), and transition optimized shifted Hermite (TOSH) methods all start with this fourth order expansion.[51–54] While all of these methods are very effective, they require the molecular geometry of interest to be well optimized using the same method and basis set as is used in the frequency calculation. These methods can be extended to include the effects of anharmonic coupling between different normal modes fairly easily, by including the appropriate third and fourth order mixed partial derivatives.[51] However, we wish to eventually compute vibrational frequencies of one specific normal mode for snapshots from molecular dynamics simulations. The molecules sampled will not necessarily even have geometries that are optimized according to the dynamical force field! Thus, we require a method for calculating the vibrational Hamiltonian which does not assume the first derivative of the potential energy is zero.

The discrete variable representation (DVR) method can also be used to compute vibrational states.[55] In this method, we again start with the normal mode vibrational Hamiltonian,

$$\hat{H} = \frac{\hat{p}_Q^2}{2\mu_Q} + \hat{V}(Q) \tag{7}$$

We then *discretize* the normal mode - we select P normal mode coordinate points $Q_1, Q_2, Q_3 \dots Q_P$ equally spaced by ΔQ to investigate. These normal mode coordinate values each represent a particular molecular geometry (Figure 1) and from them we form a grid across the normal mode coordinate.

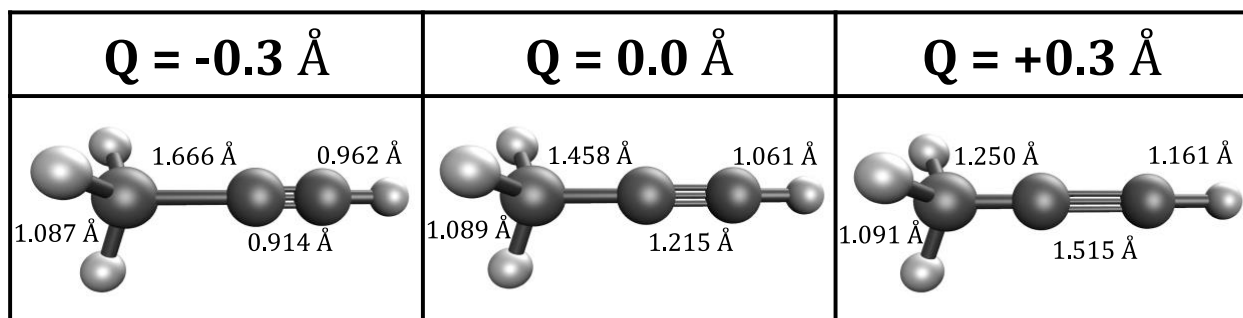| Q = -0.3 Å	Q = 0.0 Å	Q = +0.3 Å
1.666 Å 0.962 Å 1.087 Å 0.914 Å	1.458 Å 1.061 Å 1.089 Å 1.215 Å	1.250 Å 1.161 Å 1.091 Å 1.515 Å

Figure 1. The CC stretch normal mode coordinate for the propyne molecule at MP2/aug-cc-pVTZ. See Eq. 2 for the definition of the normal mode coordinate, Q . Per that definition, $Q = 0.0$ Å corresponds to the optimized structure of the molecule. Other values of Q correspond to different molecular structures. For example, $\frac{\partial r_{C \equiv C}}{\partial Q}$ is positive. Because of this, the C≡C bond length is larger than optimum when Q is positive and is smaller than optimum when Q is negative.

Under the Born-Oppenheimer approximation, the potential energy at a particular grid point is the energy of nuclear repulsion plus the ground state electronic energy for that atomic configuration,

$$V(Q_i) = \sum_{j=1}^{N} \sum_{k>j}^{N} \frac{Z_j Z_k}{R_{jk}(Q_i)} + \langle \psi(Q_i)|\hat{h}(Q_i)|\psi(Q_i)\rangle \tag{8}$$

where N is the number of atoms in the molecule, Z_j is the charge of nucleus j , $R_{jk}(Q_i)$ is the distance between atoms j and k at normal mode grid point i , $|\psi(Q_i)\rangle$ is the ground state electronic wavefunction at normal mode grid point i , and $\hat{h}(Q_i)$ is the electronic Hamiltonian at normal mode grid point i .[50] This expression defines a Born-Oppenheimer potential energy surface (PES). Once the PES at the grid points has been collected, the vibrational Schrödinger equation can be solved. Because our PES information has been collected specifically at the grid points, we expand our vibrational eigenstates in a basis of grid point position eigenfunctions, $|Q_i\rangle$.[55] This basis has the following properties:

$$\langle Q_i|Q_j\rangle = \delta_{ij} \tag{9}$$

$$\langle Q_i | \hat{Q} | Q_j \rangle = Q_i \delta_{ij} \tag{10}$$

$$\langle Q_i | \hat{V}(Q) | Q_j \rangle = V(Q_i) \delta_{ij} \tag{11}$$

where Q_i is the value of the normal mode coordinate at grid point i, and δ_{ij} is the Kronecker delta function. In this basis, the normal mode position operator and functions of that operator are diagonal. There are several ways to define such a basis, but this property is central to the DVR method.[55–58] Given such a basis, it can be shown that (in atomic units)[55,56,58]

$$\left\langle Q_i \left| \frac{\hat{p}_Q^2}{2\mu_Q} \right| Q_j \right\rangle = \frac{(-1)^{i-j}}{2\mu_Q \Delta Q^2} \begin{cases} \dfrac{\pi^2}{3}, & i = j \\ \dfrac{2}{(i-j)^2}, & i \neq j \end{cases} \tag{12}$$

This result is only exact in an infinite basis of grid points and grid point position eigenfunctions (i.e. when $P \to \infty$ and $\Delta Q \to 0$) with infinite extent (i.e. $Q_1 \to -\infty$ and $Q_P \to \infty$).[55,57,58] However, in most cases, the kinetic energy converges so long as the grid spacing ΔQ is less than about 10 pm, the number of grid points P is greater than about 10, and the extent is large enough that $\hat{V}(Q_1)$ and $\hat{V}(Q_P)$ are each at least 10 × the energy spacing from the harmonic oscillator approximation.[56,57,59–64] With this, we can construct the vibrational Hamiltonian matrix as

$$\hat{H}_{ii'} = \langle Q_i | \hat{H} | Q_j \rangle = \left(\frac{(-1)^{i-j}}{2\mu_Q \Delta Q^2} \begin{cases} \dfrac{\pi^2}{3}, & i = j \\ \dfrac{2}{(i-j)^2}, & i \neq j \end{cases} \right) + V(Q_i) \delta_{ij} \tag{13}$$

Note that because the $|Q_i\rangle$ are not vibrational eigenfunctions, the vibrational Hamiltonian matrix should generally not be diagonal in their basis. Upon diagonalization of the Hamiltonian, we obtain the vibrational eigenvalues, E_a, and eigenstates, $|\Psi_a\rangle$. The vibrational eigenstates can be represented as weighted sums of the original grid point basis functions

$$|\Psi_a\rangle = \sum_{i=1}^{P} e_{ia} |Q_i\rangle \tag{14}$$

where e_{ia} is the weighted contribution of $|Q_i\rangle$ to eigenstate $|\Psi_a\rangle$. The absolute square of each e_{ia} is the probability of the molecule having normal mode coordinate value Q_i if it is in eigenstate Ψ_a, i.e. $p_a(Q_i) = |e_{ia}|^2 = e_{ia}^* e_{ia}$. These eigenstates are orthonormal

$$\langle \Psi_a | \Psi_b \rangle = \sum_{i=1}^{P} \sum_{j=1}^{P} e_{ia}^* e_{jb} \langle Q_i | Q_j \rangle = \sum_{i=1}^{P} e_{ia}^* e_{ib} = \delta_{ab} \tag{15}$$

and we can use them to calculate normal mode expectation values. For example, the expectation of the position would be given by

$$\langle Q \rangle_a = \langle \Psi_a | \hat{Q} | \Psi_a \rangle = \sum_{i=1}^{P} \sum_{j=1}^{P} e_{ia}^* e_{ja} \langle Q_i | \hat{Q} | Q_j \rangle = \sum_{i=1}^{P} |e_{ia}|^2 Q_i = \sum_{i=1}^{P} p_a(Q_i) Q_i \qquad (16)$$

The vibrational eigenstates can also be used to calculate useful vibrational properties such as the transition dipole moment and the isotropic transition polarizability. The transition dipole moment $\vec{\mu}_{ab}$ is related to the probability of absorption in infrared spectroscopy experiments and can be computed as

$$\vec{\mu}_{ab} = \langle \Psi_a | \vec{\mu}(Q) | \Psi_b \rangle = \sum_{i=1}^{P} \sum_{j=1}^{P} e_{ia}^* e_{jb} \langle Q_i | \vec{\mu}(Q) | Q_j \rangle = \sum_{i=1}^{P} e_{ia}^* e_{ib} \vec{\mu}(Q_i) \qquad (17)$$

where $\vec{\mu}(Q)$ is the three-dimensional dipole moment surface along the normal mode; the $\vec{\mu}(Q_i)$ are the molecular dipole moments at each of our P grid points.[25,65,66] The isotropic transition polarizability α_{ab} is related to the probability of isotropic Raman scattering and can be computed as

$$\alpha_{ab} = \langle \Psi_a | \hat{\alpha}(Q) | \Psi_b \rangle = \sum_{i=1}^{P} \sum_{j=1}^{P} e_{ia}^* e_{jb} \langle Q_i | \hat{\alpha}(Q) | Q_j \rangle = \sum_{i=1}^{P} e_{ia}^* e_{ib} \alpha(Q_i) \qquad (18)$$

where $\alpha(Q)$ is the trace of the polarizability tensor surface along the normal mode,

$$\alpha(Q) = \frac{\alpha_{xx}(Q) + \alpha_{yy}(Q) + \alpha_{zz}(Q)}{3} \qquad (19)$$

and can be collected at each of our P grid points.[65,67] Diagonalization of the vibrational Hamiltonian also produces a series of eigenvalues which we interpret as energy levels. The frequency of light resonant in a transition from vibrational state a to state b is

$$\omega_{ab} = \frac{E_b - E_a}{h} \qquad (20)$$

where E_a is the energy of state $|\Psi_a\rangle$ and h is Plank's constant.

III. Computational Methods:

I. Electronic Structure Methods and Basis Sets.

The quantum chemistry methods employed in this study include Hartree-Fock (HF)[68], the post-Hartree-Fock methods MP2[69] and CCSD(T)[70], and density functional theory (DFT) methods

spanning several rungs of "Jacob's ladder": B3LYP-D3[71–74], ωB97M-V[75], TPSS-D3[74,76], and PBEh-3c[77]. The comparison of HF to other methods allows us to understand the effect of exact exchange and the other method's approximate electron correlation on the frequency calculation. We use CCSD(T) as a "gold standard" electronic structure method, and MP2 as a sort of "silver standard" - not as accurate as CCSD(T) yet still reasonably applicable to some of the larger molecules examined in this study, and more accurate than DFT. We select TPSS-D3, B3LYP-D3, and ωB97M-V as representative, widely used, and economical meta-GGA, global hybrid GGA, and range-separated hybrid meta-GGA functionals, respectively, with recommended empirical dispersion corrections. The composite method PBEh-3c (with the recommended def2-mSVP modified basis set) is included because of its impressive cost to accuracy ratio. These choices were influenced by recommendations from the quantum chemistry community, as were our basis set choices.[78–80] This search will allow us to find an economical method to use for our future condensed phase frequency calculations while uncovering some of the quantum effects on the frequency.

We also tested the effect of the basis set on the frequency by examining three families of basis sets: Pople, Dunning, and Ahlrichs.[81–83] For each family, basis sets of the same zeta quality and with the same presence of diffuse functions were tested. The four combinations were: (1) double zeta with no diffuse functions [6-31G**, cc-pVDZ, and def2-SVP], (2) double zeta with diffuse functions on all atoms [6-31++G**, aug-cc-pVDZ, and def2-SVPD], (3) triple zeta with no diffuse functions [6-311G**, cc-pVTZ, and def2-TZVP], and (4) triple zeta with diffuse functions on all atoms [6-311++G**, aug-cc-pVTZ, and def2-TZVPD]. Because we will eventually calculate Raman intensities which are strongly dependent on polarization effects, we always include polarization functions on all atoms in our basis sets. For CCSD(T) and MP2, each of the largest triple zeta basis sets [6-311++G**, aug-cc-pVTZ, and def2-TZVPD] were used in order to obtain values with high accuracy for comparison to other methods.

II. Molecular Analysis

All geometry optimizations, harmonic frequency calculations, single point energy calculations, and polarizability calculations were performed using the Q-Chem 5.4 software package.[78] Single point energy calculations were typically performed using an self-consistent field (SCF) convergence criterion of 10^{-9} atomic units and a threshold for the neglect of two electron integrals of 10^{-14} atomic units. The relaxed constraint algorithm was used during early SCF iterations, and the Pulay DIIS algorithm was used during later iterations.[84,85] For DFT calculations a quadrature grid with 99 radial points and 590 angular points was used, but a lower resolution SG-0 grid was used for early SCF cycles.[86] We attempted to optimize all molecular geometries to a maximum gradient of 3×10^{-6} atomic units; if this was not possible, the restriction was loosened to 30×10^{-6} atomic units. Optimization was confirmed by the absence of imaginary harmonic frequencies. Dipole moments were computed analytically based on the ground state electronic wavefunction and static polarizability tensors were computed using the finite field approach. Both computations were completed using the appropriate Q-Chem implementation.[78]

We investigated four classes of alkyne containing molecules. These included small alkynes with carbon-based R groups, small alkynes with non-carbon substituents, large alkynes, and synthetic amino acids. The synthetic amino acids were examined in their fully neutral forms, since those forms are the most stable in the gas phase.[87,88] We performed shorter DFT analyses on the zwitterionic forms and found no evidence that our results would be different if we'd

examined these forms. These choices were inspired by the work of Romei et al. and allow us to investigate a diverse array of alkyne containing molecular structures.[38]
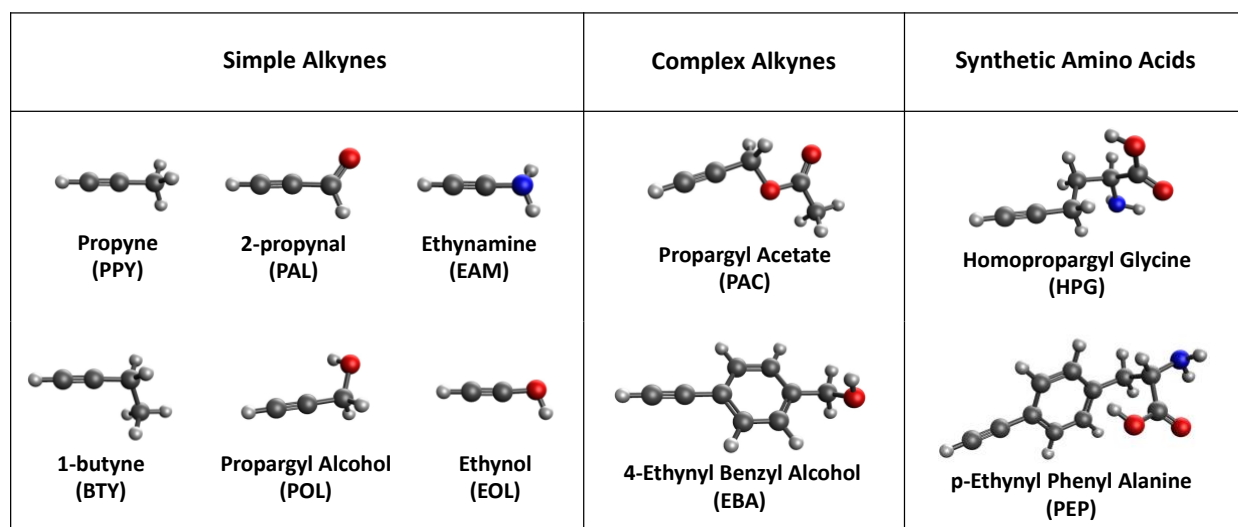

Figure 2. Terminal alkyne molecules examined in this study. These optimized geometries were obtained using MP2/aug-cc-pVTZ. The three letter codes in parentheses are used throughout this work to refer to the molecules they appear underneath.

III. Localized Vibrational Frequency Calculations.

While the molecules we're investigating vary by R group, the atoms of the terminal alkyne moiety (-C≡C-H, hereafter CCH) are common between them. These atoms have much larger displacements in the CC triple bond normal mode motion than the other atoms in each molecule (see Figure 1 and section IV.B.3. on localization error). Physically, this means the non-CCH atoms barely move during the vibration. One common approximation which can simplify a normal mode substantially is *localization*.[89–94] In our localization approximation, we remove the motion of all non-CCH atoms in the molecule during the vibration so that only the CCH atoms move.

We do this in two separate but similar ways. In one method, we use the partial Hessian approximation.[95,96] Here, the masses of non-CCH atoms are assumed to be so large that their mass-weighted Hessian entries can be neglected. This results in different values of the normal mode displacements than when the full mass-weighted Hessian is diagonalized. These displacements can be used to compute the reduced masses, scan the potential energy surface, and perform any other tasks that their full Hessian counterparts are used for in our DVR method. The second way we can localize the normal mode is by simply setting the non-CCH atom displacements to zero, and using the full Hessian CCH displacements as in the partial Hessian case. Both of these methods result in similar DVR localized normal mode frequencies, reduced masses, and CCH displacements (Table S1). We preferred the partial Hessian-based method of localization if it was available in Q-Chem. Of the methods we explored, it is only unavailable for CCSD(T).

IV. Results and Discussion

Section 1. Performance of the Isolated Normal Mode DVR Method

Subsection A. Overall Performance

We performed anharmonic frequency calculations using the established VPT2 method implemented in the Q-Chem package with the "gold standard" CCSD(T) electronic structure method and triple zeta basis sets with diffuse functions to obtain benchmark anharmonic CC stretch frequencies. Experimental values for all molecules are taken from NIST sources.[97–103] Nyquist reports 2185 cm^{-1} for the CC stretch frequency for POL.[104] However, this disagrees with several other sources for the vapor and condensed phase frequency of this molecule, including the pictured spectrum in the Nyquist reference itself.[38,97,104–107] Because of the disagreement with all other sources and our otherwise highly accurate CCSD(T)/triple zeta/VPT2 calculations, we believe this is a misreport and that sources stating the frequency is 2124 cm^{-1} are correct. We show in Table 1 that the calculated frequencies using VPT2 are within 10 cm^{-1} of the experimental frequency for most of our small molecules. We were not able to complete a VPT2 calculation for BTY/CCSD(T)/aug-cc-pVTZ because of the large memory and time requirements of the calculation. We observe a small basis set dependence on the calculated frequencies, and find that the Dunning and Alrichs family basis sets are most consistent with the reported experimental gas-phase frequency.

VPT2 is known to fail catastrophically in cases where two or more vibrational transitions have nearly the same energy, so it is important to check if such transitions exist before using the method.[51,53] We have checked this using the transition-optimized shifted Hermite (TOSH) method. TOSH is an approximation to VPT2 and does not share the concern of catastrophic failure.[51] Because VPT2 and TOSH calculations are automatically performed simultaneously in Q-Chem, we have values from both methods for every calculation we performed. The frequencies we obtain from the TOSH method are always similar to those we obtain from VPT2, with an RMSD of 3.6 cm^{-1} (see Figure S1). This is strong evidence that the VPT2 method is not suffering from catastrophic failure for the CC stretch. In the absence of these failures, the VPT2 calculations have the best cost to accuracy ratio of the anharmonic vibrational frequency methods packaged with Q-Chem.[78] As such, we use VPT2 anharmonic frequency calculations as a benchmark against which to test our localized DVR anharmonic frequency calculations.

We tested the performance of our localized normal mode DVR method against VPT2. CCSD(T) was used for both calculations; using such an accurate electronic structure method allows us to isolate inaccuracies due to the vibrational method alone. The DVR method nearly matches the performance of the VPT2 method for the small molecules where the atom directly bonded to the alkyne group is a carbon. However, the DVR frequencies for EOL and EAM differ substantially from experiment and VPT2. The calculated DVR frequencies are compared to experiment and VPT2 frequencies in Table 1.

Table 1: Difference of calculated CC stretch frequencies from reported experimental gas phase frequencies for our set of six small terminal alkyne molecules. All frequencies are reported in cm^{-1} as $\Delta\omega = \omega_{calc} - \omega_{exp}$.

RMSD $= \sqrt{\frac{1}{n}\sum_{i=1}^{n}(\Delta\omega_i)^2}$, where i iterates over each unique molecule. The RMSD is given for only molecules

	Expt	aug-cc-pVTZ		def2-TZVPD		6-311++G(d,p)	
		VPT2	DVR	VPT2	DVR	VPT2	DVR
PPY	2124	+2	+4	+13	+6	+2	-6
PAL	2125	-19	-17	-8	-16	-31	-28
BTY	2116	--	+8	+16	+8	-6	-2
POL	2124	-3	+1	-1	+1	-11	-8
EAM	2155	-2	-29	-4	-17	-1	-37
EOL	2198	-11	-39	-19	-28	-20	-43
RMSD$_{R=C}$	--	11	10	11	9	17	15
RMSD$_{all}$	--	10	21	12	15	16	26

Subsection B. Sources of Error

Our localized normal mode DVR method makes three major assumptions about the terminal alkyne CC vibration: (1) that the error of discretizing the potential energy surface is negligible, (2) that the CC stretch normal mode is not anharmonically coupled to other normal modes in the molecule, and (3) that the atoms in the R group do not move during the vibration. All of these are formally incorrect. In the following, we investigate each of these assumptions to determine the amount of error they introduce to our method.

1. Is the error from discretizing the potential energy surface negligible?

The true potential energy surface for the normal mode is continuous ($P \to \infty$ and $\Delta Q \to 0$) and has an infinite domain ($Q_1 \to -\infty$ and $Q_P \to \infty$). However, our DVR method discretizes and limits this surface, and these approximations introduce some error. To determine this error, we produced a DVR potential energy surface with a very fine grid ($P = 100$ and $\Delta Q = 0.02$ Å) and a very large domain ($Q_1 = -1.0$ Å and $Q_{100} = 1.0$ Å) at the MP2/aug-cc-pVTZ level of theory for propyne (Figure 3). The ω_{01} DVR frequency obtained using this PES was 2114.53 cm^{-1}. To ensure that this value was converged with respect to the number of grid points and the domain, PES grids with reduced resolution and domain were produced and used to compute the ω_{01} DVR frequency. No change greater than 0.2 cm^{-1} was observed until the grid spacing, ΔQ, was increased to more than 0.04 Å. Also, the 100 grid point PES DVR results reproduce the behavior expected of a slightly anharmonic oscillator (Figure 3); the energy level spacing decreases slowly as the energy eigenvalue increases, and the high energy wavefunctions are highly oscillatory. Thus, we believe it is reasonable to treat this 100 grid point PES as nearly continuous and nearly unlimited.

We compared this nearly continuous and nearly unlimited surface to our preferred surface, containing $P = 20$ grid points between $Q_1 = -0.3$ Å and $Q_{20} = 0.5$ Å ($\Delta Q = 0.04$ Å). The ω_{01} frequency obtained using the near-continuous PES (2114.53 cm^{-1}) is consistent with the calculated ω_{01} frequency using the 20 grid point PES (2114.72 cm^{-1}). This happens because the low energy eigenvalues for both PESs are very similar (Figure 3). The high energy eigenstates

obtained from the 20 grid point PES are not similar to those from the near continuous surface, indicating increasing error with increasing energy. The 20 grid point PES would be inadequate to compute, say, the ω_{09} frequency. However, we are most interested in the ω_{01} frequency and the error from discretization for this value is 0.19 cm^{-1}. We find this error is acceptable in exchange for computing one-fifth as many PES grid points.
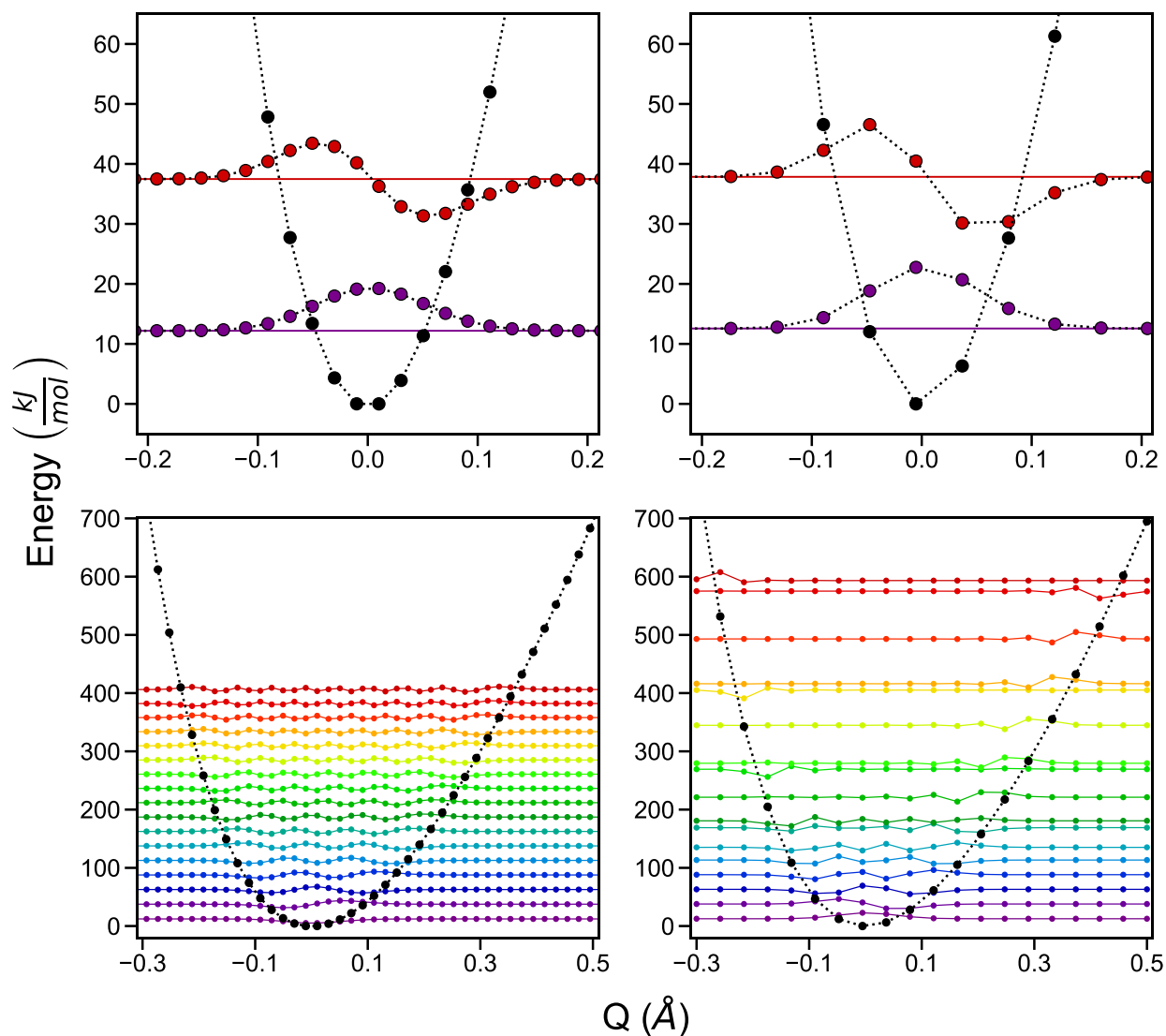

Figure 3. Discretized PES for propyne (MP2/aug-cc-pVTZ) with 100-point (left) and 20--point (right) grids. The top panels demonstrate that the two grids produce essentially identical vibrational wavefunctions and energy levels for the ground and first excited vibrational states. The bottom panel shows that the vibrational states, which are drawn at their respective energy levels, diverge between the two grids at igh energies. The vibrational states of the nearly continuous 100--point grid show the behavior one would expect of a slightly anharmonic oscillator.

2. Is the CC stretch normal mode only weakly anharmonically coupled to other normal modes in the molecule?

Molecular normal modes are completely orthogonal motions of a molecule under the harmonic oscillator approximation (this is, in fact, the definition of a normal mode). However, normal modes generally mix with other normal modes once anharmonicity is considered. Our DVR method implicitly assumes that the CC stretch normal mode is *anharmonically isolated*. To determine the error due to this assumption, which we term e_{iso}, we performed anharmonic VPT2 frequency calculations for the isolated CC stretch normal mode. In this calculation, 3rd and 4th derivatives of the energy are only computed with respect to the CC stretch normal mode; no other anharmonic normal mode information is included in the calculation. In effect, this anharmonically isolates the CC stretch vibration in a similar way to our DVR method. e_{iso} is approximated as the difference between the isolated VPT2 value and the VPT2 frequency with normal mode coupling using CCSD(T) and triple zeta basis sets (i.e. $\omega_{\mathrm{iso}} - \omega_{\mathrm{coup}}$). The error due to normal mode isolation is reported in Table 2, and the average e_{iso} is +40 cm^{-1}.

Table 2: e_{iso} is calculated as the difference between isolated and ordinary VPT2 frequency calculations using CCSD(T) and a series of triple zeta basis sets. CC stretch normal mode isolation results in a higher calculated frequency by an average of +40 cm^{-1}. The individual frequencies are given in the SI.

	aug-cc-pVTZ	def2-TZVPD	6-311++G(d,p)
PPY	+37	+40	+30
PAL	+27	+29	+29
BTY	--	+38	+37
POL	+33	+45	+34
EAM	+42	+43	+35
EOL	+44	+51	+51

The total anharmonicity of the CC stretch normal mode can be approximated as the difference between harmonic and VPT2 frequencies (i.e. $\omega_{\mathrm{harm}} - \omega_{\mathrm{coup}}$) using the same CCSD(T) electronic structure theory. A strong correlation between e_{iso} and the total anharmonicity indicates that a significant portion of the variance in the total anharmonicity is due to normal mode coupling, rather than *isolated* normal mode anharmonicity (harmonic frequency calculations do not capture either effect). We find a moderately strong correlation (R=0.80, p < 2 x 10^{-3}) between e_{iso} and the overall anharmonicity (Figure 4). A linear regression treating the approximate total anharmonicity as the independent variable has a slope of 0.84, quite close to 1. This, and the small y-intercept value of 3.3 cm^{-1}, implies that a large portion of the overall magnitude of the anharmonicity (not just its variation) is due to normal mode coupling – if the slope were exactly 1, we could essentially say $e_{\mathrm{iso}} = \omega_{\mathrm{harm}} - \omega_{\mathrm{coup}}$. This follows from the fact that the isolated CC stretch normal mode vibration itself is fairly harmonic (see Figure 3). Figure 4 also shows that few of the molecules strongly tend to reliably have higher or lower anharmonicity across all basis sets, leading to the relatively constant e_{iso} seen in Table 2.
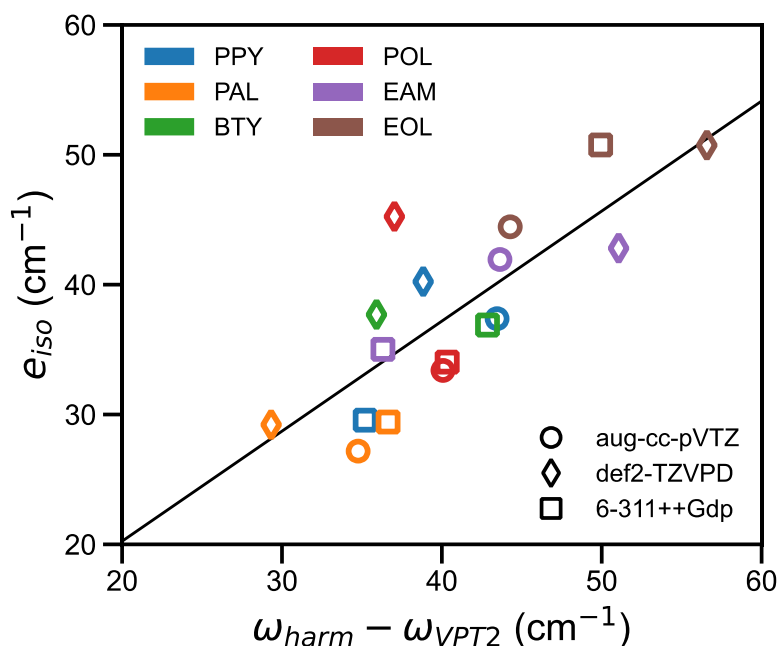
Figure 4. Correlation between approximate total anharmonicity (horizontal axis) and isolation error (vertical axis). The best fit line is in black (R = 0.80, p < 2 x 10⁻³).

3. Do the R group atoms move only a small amount during the vibration?

Our localization method makes the approximation that only the CCH atoms move during the vibration. This cannot be exactly true – a pure vibration would not translate or rotate the molecule, but a CCH-only vibration would. This could be partially resolved by satisfying the appropriate Eckart conditions at each grid point.[108] Unfortunately, our method cannot rely on satisfying these conditions in order to be truly universal – as the systems we investigate become larger, the conditions would become more difficult to satisfy. Consider, say, a terminal alkyne moiety covalently bonded to a protein.[39] What effect does removing the R group displacement have on the normal mode motion and frequency, and is mixing translation and rotation into the vibration acceptable?

To quantify the effect on the motion we analyzed the atomic normal mode displacements reported by harmonic frequency calculations for all small probes using CCSD(T) with the same series of basis sets. We found that on average the magnitude of the R group atom displacement is 0.071 Å while the average magnitude of ≡**C**-R, ≡**C**-H, and ≡C-**H** atom displacements were 0.559 Å, 0.385 Å, and 0.719 Å, respectively. The R group motion for EAM and EOL is larger, averaging 0.120 Å. The much larger CCH displacements show that these atoms are the most important in the vibrational mode. We used harmonic MP2/aug-cc-pVTZ calculations to quantify the localization error for our larger molecules (PAC, EBA, PEP, HPG), some of which exhibit strong pi-conjugation between the terminal alkyne and moiety and an aromatic ring. Localization is strong for these molecules as well. The average magnitude of R group atom displacement is 0.019 Å while the average magnitude of ≡**C**-R, ≡**C**-H, and ≡C-**H** atom displacements were 0.570 Å, 0.391 Å, and 0.709 Å, respectively. At MP2/aug-cc-pVTZ, the same values for the six small probes are

very similar, at 0.571 Å, 0.388 Å, and 0.707 Å, respectively. Even when pi-conjugation is present, the C≡C stretch vibration is local to the CCH atoms.

We also quantified the effect on the calculated frequencies. We performed both harmonic and DVR frequency analyses that capture the error due to localizing the vibration to the CCH atoms. Specifically, we compared full harmonic frequencies to localized harmonic frequencies, and separately we compared full normal mode DVR frequencies to localized normal mode DVR frequencies. The localized harmonic frequencies were computed using the numerical second derivative of the energy as a function of the localized normal mode coordinate near $Q = 0$. All of these frequency calculations were performed using the CCSD(T) method with the same series of basis sets as above.

Table 3: The error due to localization is determined using harmonic and anharmonic approaches, CCSD(T) electronic structure theory, and a series of triple zeta basis sets. Localization decreases the calculated frequency by about 43 cm^{-1}. The effect of localization is highest for molecules where the R group is not carbon based. The individual frequencies are given in the SI.

	aug-cc-pVTZ		def2-TZVPD		6-311++G(d,p)	
	harm	anharm	harm	anharm	harm	anharm
PPY	-30	-37	-31	-36	-36	-39
PAL	-26	-26	-22	-26	-21	-28
BTY	-32	-33	-30	-33	-33	-35
POL	-28	-31	-16	-31	-25	-33
EAM	-70	-70	-66	-69	-68	-72
EOL	-67	-73	-68	-72	-68	-74

The error due to localization, e_{loc}, was estimated as the difference between the isolated normal mode frequency and the full normal mode frequency (i.e. $\omega_{loc} - \omega_{full}$) for each vibrational structure method. The individual e_{loc} values are reported in Table 3. The average harmonic e_{loc} is –41 cm^{-1} and the average anharmonic e_{loc} is -45 cm^{-1}. The overall average is -43 cm^{-1}. We find that the magnitude of e_{loc} is strongly correlated to the sum of the mass-weighted displacements of the R group atoms in the full normal mode (Figure 5). In particular, the molecules with non-carbon-based R groups, EAM and EOL, have particularly large R group displacements and thus large localization errors. When they're removed from the estimate of e_{loc}, it shrinks to -30 cm^{-1} for terminal alkynes with carbon-based R groups. That this correlation exists, is strong, and is negative, shows that molecules which more fully satisfy the partial Hessian assumption of zero R group motion will have less localization error, as might be expected. The average value of the localization error for the large probes (PAC, EBA, PEP, HPG) based on harmonic MP2/aug-cc-pVTZ calculations is -18 cm^{-1} (standard deviation of 2 cm^{-1}) compared to -21 cm^{-1} (standard deviation of 7 cm^{-1}) for the six small probes at MP2/aug-cc-pVTZ. From this data, it does not seem that pi-conjugation changes the localization error.
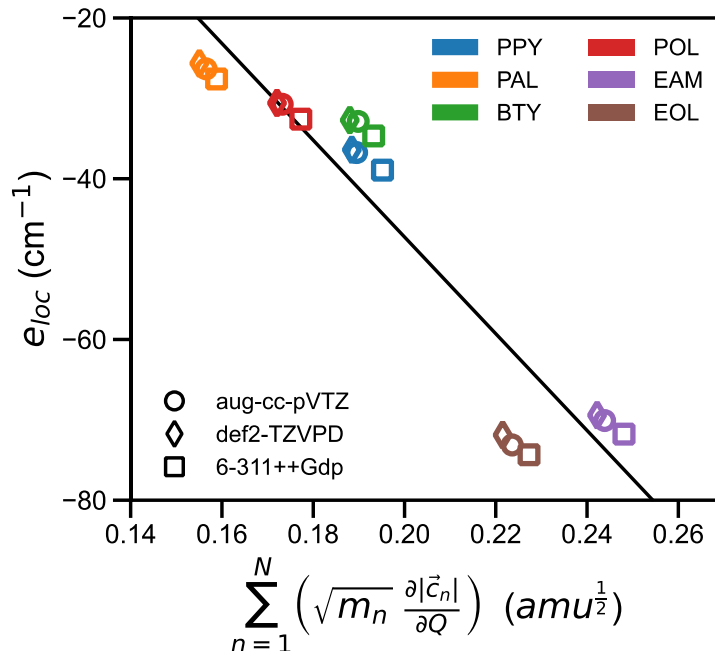
Figure 5: Correlation between the sum of the magnitude of mass-weighted displacements for all R group atoms (horizontal axis) and localization error (vertical axis). The best fit line is in black (R = -0.94, p < 1x10⁻⁸).

4. Fortuitous error cancellation:

In our localized normal mode DVR method, the error due to discretization is negligible. The errors due to isolation, $e_{iso} \approx +40$ cm^{-1}, and localization, $e_{loc} \approx -43$ cm^{-1}, are more substantial (though not individually enormous). Fortunately, they are nearly equal in magnitude and opposite in sign. This cancellation occurs not only on average across molecules and basis sets but also for most individual combinations of molecule and basis set, as depicted in Figure 6. This error cancellation is consistent across alkynes with carbon-based R groups. As shown in Figure 6, the co-cancellation of these errors explains the high accuracy of our isolated normal mode DVR method. Statistical t-tests reveal that our DVR method calculates frequencies that are indistinguishable from those calculated by the more expensive VPT2 vibrational method for molecules where the sum of the localization error and the isolation error is indistinguishable from zero. The DVR frequencies are distinct from VPT2 frequencies for molecules like EAM and EOL due to significant R group motion and high localization error.

Because of the consistency of this error cancellation, the modest magnitudes of the errors, and the resulting accuracy, we believe it is appropriate to use this method for future alkyne frequency analyses. However, anyone using this method or a similar one should check that the error cancellation remains in their context, perhaps using the comparisons we have employed above. This method would need to be more carefully adjusted for use with alkynes having non-carbon-based R groups exhibiting sigma induction since, in their case, the error does not cancel out. The effects of pi-conjugation and sigma induction on localization and anharmonic isolation for the C≡C stretch will be more carefully assessed in future work. However, it is already apparent that sigma induction in EAM and EOL changes the balance between the two sources of error. As

described above, we found that localization was an appropriate approximation for our larger pi-conjugated probes.
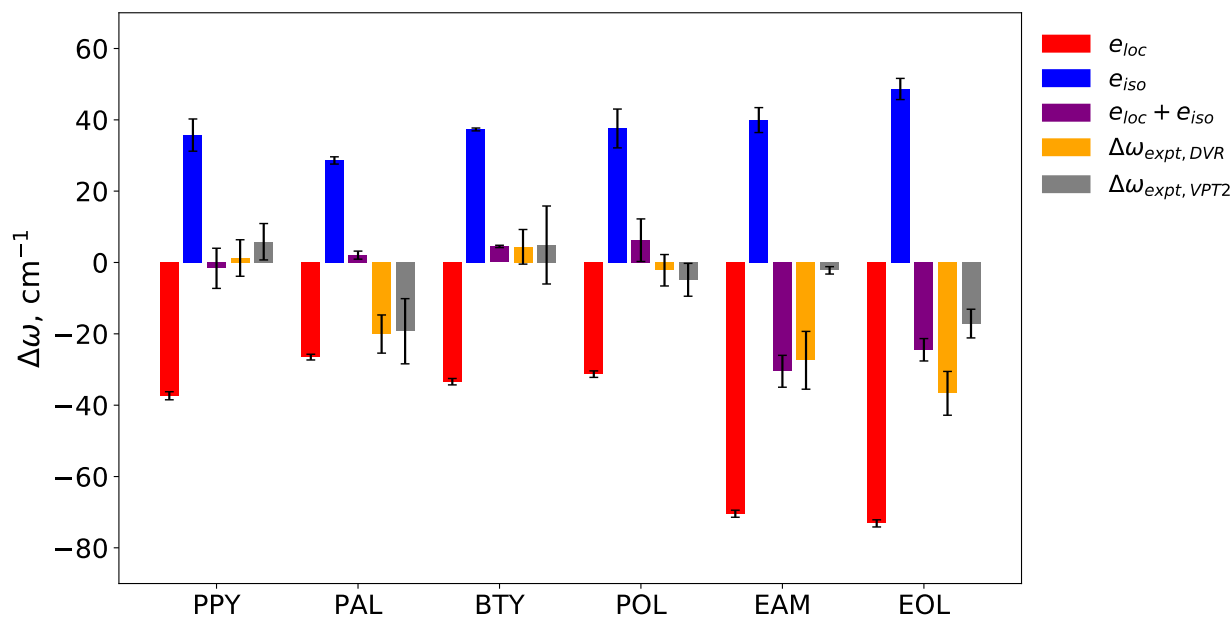

Figure 6. Decomposition and quantification of localization and anharmonic isolation errors. The performance of DVR and VPT2 calculations with respect to experiment are also included. Each value reflects an average for the series of TZ basis sets, and error bars are standard deviations. For all except PAL, the error sum ($e_{\mathrm{loc}} + e_{\mathrm{iso}}$) is indistinguishable from the DVR error ($p > 0.05$). For PPY, PAL, BTY, and POL, the DVR error is indistinguishable from the VPT2 error ($p > 0.05$) and the error sum ($e_{\mathrm{loc}} + e_{\mathrm{iso}}$) is indistinguishable from 0 ($p > 0.05$).

Section 2. Density Functional Theory Calculations

CCSD(T) is a highly accurate electronic structure method. However, it is not accessible for use with our larger probes. In the future, we would prefer to use DFT methods because of their high speed and reasonable accuracy. We use the MP2 electronic structure method as a 'silver standard' to evaluate the performance of various cheaper DFT methods. Lowering the level of theory to MP2 changes the frequency by about by an average of 4 cm^{-1} and an RMSD of 22 cm^{-1} for our small probes (values in SI).

We also calculated localized normal mode DVR frequencies using four density functionals: PBEc-3h, TPSS-D3, B3LYP-D3, and ωB97M-V. These calculations were performed using Pople, Dunning, and Alrichs style basis sets fitting the descriptions "double zeta," "double zeta with diffuse functions," "triple zeta," and "triple zeta with diffuse functions." An exception was PBEc-3h which was only used with the def2-mSVP basis set.

We used these values to compute scaling factors following Irikura et al.[109] Scaling factors are commonly used to correct for the inaccuracies in harmonic frequency calculations, which can broadly be sorted into two types. The first type of error is at the level of the vibrational calculation, especially the neglect of anharmonic effects. This is fundamental to the harmonic method. Our DVR calculations do not have this same error but, as discussed above, our approximations

introduce their own vibrational calculation errors. The second type is at the electronic structure level, where inadequacies in the description of electrons can introduce error. Because of this, scaling factors are sensitive both to the electronic structure method and the basis set. A scaling factor, c, can be computed using the formula,

$$c = \frac{\sum_i x_i z_i}{\sum_i x_i^2} \tag{21}$$

where the sum is over different molecules in the "training set" for the scaling factor, x_i are their computed frequencies, and z_i are their experimental frequencies. The uncertainty in the scaling factor is given by

$$u(c) = \left(\frac{\sum_i x_i^2 \left(\frac{z_i}{x_i} - c \right)^2}{\sum_i x_i^2} \right)^{\frac{1}{2}} \tag{22}$$

where c is the previously computed scaling factor.[109] MP2 scaling factors and their uncertainties were computed for the set of small molecules for which experimental values are available. The average MP2 scaling factor across basis sets was 1.004 ± 0.003. These scaling factors were used to predict experimental values for the larger probes where we did not have experimental data. The predicted experimental values (i.e. scaled MP2 values) are given in Table 4.

Table 4. Predicted experimental gas phase frequencies (cm^{-1}) from on localized normal mode DVR using MP2 and scaling factors obtained from the smaller probes.

	aug-cc-pVTZ	def2-TZVPD	6-311++G(d,p)	Average
PAC	2131	2132	2138	2134
EBA	2099	2094	-	2097
HPG	2115	2117	2114	2115
PEP	2100	2100	2098	2099

The averages of these predicted experimental values were used along with authentic experimental values for the small probes to compute scaling factors and uncertainties for all the density functional methods (Figure 7). The results are nearly identical to those obtained if only the small probes with true experimental frequencies are used. If EAM and EOL are removed from the training set, the uncertainties become smaller but the magnitudes of the scaling factors remain nearly the same.
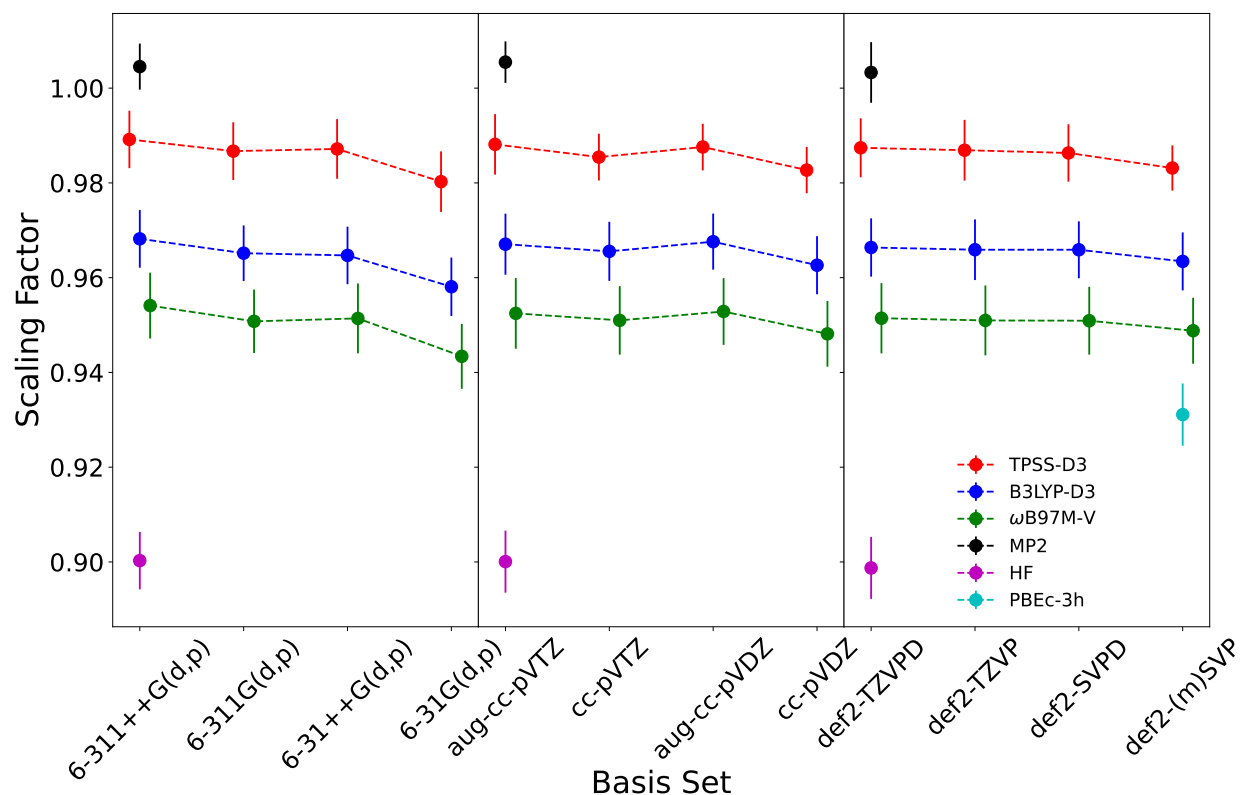
Figure 7. Estimated scaling factors for different combinations of basis set and electronic structure method. Frequencies were calculated using the localized normal mode DVR method developed in this work. For PBEc-3h, the def2-mSVP basis set was used. This basis set is a slightly modified version of the def2-SVP basis set, which was used for the other density functionals.

A vibrational frequency method with no vibrational or electronic sources of error would have a scaling factor of 1.0. By this metric, MP2 performs very well, and so serves as an effective benchmark. HF performs relatively poorly with an average scaling factor of 0.900 ± 0.003, showing that electron correlation is an important factor in these calculations. Contrary to our prior expectations, TPSS-D3 is the cheapest *and* most accurate DFT method for calculating the terminal alkyne CC stretch frequencies. The best scaling factor was 0.989 ± 0.006 for TPSS-D3/6-311++G(d,p). ωB97M-V has surprisingly poor performance, though even its lowest scaling factor of 0.943 ± 0.007 for ωB97M-V/6-31G(d,p) is fairly reasonable. PBEc-3h/def2-mSVP has the worst performance of the density functionals at a scaling factor of 0.931 ± 0.007. All methods and all basis set families show a marked improvement in the frequency predictions when going from a double zeta basis set to a double zeta basis set with added diffuse functions. For the Pople and Dunning basis set families, performance is worsened whenever diffuse functions are removed, while the double/triple zeta distinction is less important. The Alrichs basis sets are more "stable" in a sense – changing the basis set features has the least effect on performance for this family. The Pople basis sets are the most erratic, so a small change in basis set character can have a large effect on performance. Based on these results, an ideal model chemistry would include a functional like TPSS-D3 and a basis set of at least double zeta quality with diffuse functions included.

One reason that TPSS-D3 may perform better than the other functionals is because it was derived from fundamental density functional theory principles, with very few fitted parameters.[76] B3LYP-D3 and ωB97M-V include several adjustable parameters which were fit based on experimental data on several (or many) smaller molecules.[71,75] The small molecule training sets did not include many alkynes or other triple bonded molecules, which may harm their ability to characterize triple bonds compared to a less empirically influenced method. Presumably, an empirical DFT method based on many triple bonded molecules would perform even better than TPSS-D3. The importance of diffuse functions in the basis set likely also comes down to the presence of the triple bond. In a triple bonded molecule, there is substantial electron density placed unusually far from the nuclei. A basis set without diffuse functions might have some difficulty fully describing this. Describing the triple bond well is particularly important when computing these CC bond frequencies which directly depend on estimating the bond strength. A deeper understanding of these trends would likely require very careful electronic structure analysis, which is outside the scope of this work.

Section 3. Properties of the Vibration

1. Transition Isotropic Polarizabilities and Transition Dipole Moments

Using this vibrational method, we can compute a number of useful vibrational properties. Here, we focus on the calculation of the transition dipole moment and the isotropic transition polarizability. To compute these, we first obtain the dipole moment and isotropic polarizability surfaces, shown in the left panels of Figure 8. These surfaces were calculated for all our molecules at the grid point structures used in our localized normal mode DVR calculations at TPSS-D3/6-311++G(d,p). The dipole moment is reported as the overlap (dot product) between the full dipole moment vector and the unit vector pointing from the carbon bonded to the R group to the carbon bonded to the terminal hydrogen. The isotropic polarizability is reported as the trace of the full polarizability tensor. In general, the projection of the dipole moment decreases slowly as the normal mode coordinate increases (note the y-axis). For the molecules where the R group does not begin with carbon, the decrease is more rapid; for PAL the dipole moment projection actually increases with the normal mode coordinate. The polarizability increases along the normal mode for all molecules; this is expected, since molecular bond lengths are generally increasing as the normal mode coordinate increases. The magnitude of this increase is generally fairly large, especially for the molecules containing aromatic rings.
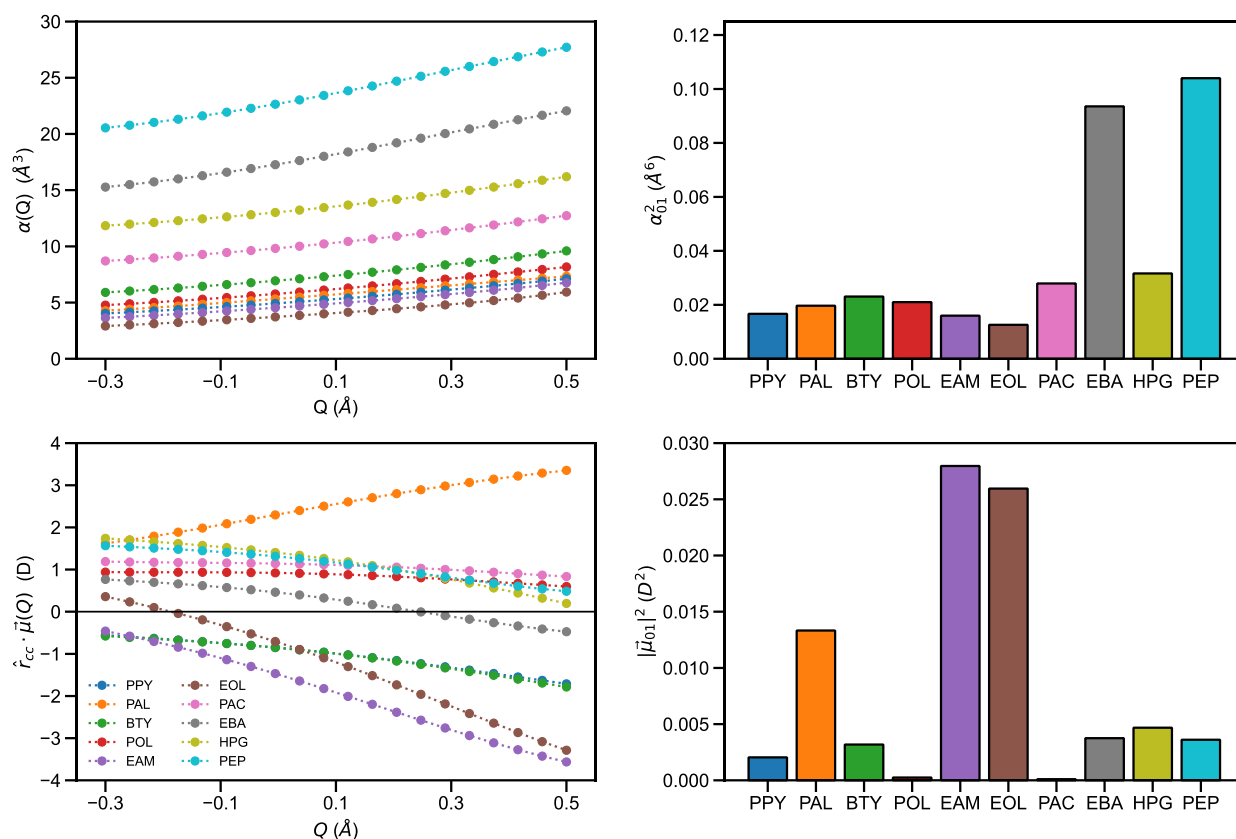
Figure 8. Isotropic polarizability (top left) and dipole moment (bottom left) surfaces as a function of the CC stretch normal mode coordinate, Q. The isotropic transition polarizability (top right) and transition dipole moment (bottom right) are computed using these surfaces and vibrational wavefunctions from our localized normal mode DVR method. All properties are calculated for each probe molecule using TPSS-D3/6-311++G(d,p).

The dipole moment and polarizability surfaces, along with our DVR vibrational wavefunctions, enable us to compute transition dipole moments and transition polarizabilities for the $|\Psi_0\rangle \rightarrow |\Psi_1\rangle$ transition. The square of the transition dipole moment is proportional to the probability of absorption in infrared spectroscopy experiments, and the square of the transition polarizability is directly related to the probability of scattering in Raman spectroscopy experiments.[65] These are shown in the right part of Figure 8. As expected, the transition dipole moments are relatively small. For comparison, the square of the transition dipole moment of the highly IR active CO_2 asymmetric stretch $|\Psi_0\rangle \rightarrow |\Psi_1\rangle$ transition is 0.106 D^2; the largest in our set of alkynes is about one-third this value at 0.0280 D^2.[110,111] The largest transition dipoles occur for the probes where the triple bond is attached to an atom which is not carbon where significant sigma induction is possible. Most of the values are much smaller. The transition polarizabilities, however, are fairly large. Again, using CO_2 as a comparator, the Raman active symmetric stretch $|\Psi_0\rangle \rightarrow |\Psi_1\rangle$ transition couples with the $|\Psi_0\rangle \rightarrow |\Psi_2\rangle$ overtone of the bending vibration which results in two strong peaks. The squared transition polarizability of the first is 2.52 x 10^{-3} A^6 and of the second is 3.73 x 10^{-3} A^6.[112] In our group of alkynes, the smallest squared transition polarizability is 12.6 x 10^{-3} A^6 and the largest is 104 x 10^{-3} A^6. The transition polarizabilities are especially large

for the alkyne molecules pi-conjugated to aromatic rings, for whom stronger Raman scattering has already been observed in experiments.[29,38]

2. Universal Displacements

The localized CCH atom displacements for the terminal alkyne CC normal mode are remarkably similar across all of the molecules observed in this study. To take advantage of this similarity, we performed localized normal mode DVR on all molecules, with all basis sets and DFT functionals described in this work. These calculations were performed twice and then compared. In the first iteration, displacements were obtained individually, so each molecule, DFT method, and basis set combination had its own specific atomic normal mode displacements. In the second iteration, the localized displacements for the CCH atoms of propyne at MP2/aug-cc-pVTZ were used for all molecules, DFT method, and basis sets. In Figure 9, the strong correlation between these two methods of displacing the CCH atoms is shown. It is clear that the atomic displacements of the CCH atoms in the CC stretch are fairly *universal* – one could switch the specific values between any pair of molecule, DFT method, and basis set combinations. In future work, we will use such universal CC displacements to simplify the calculation of terminal alkyne vibrational frequencies from molecular dynamics snapshots.
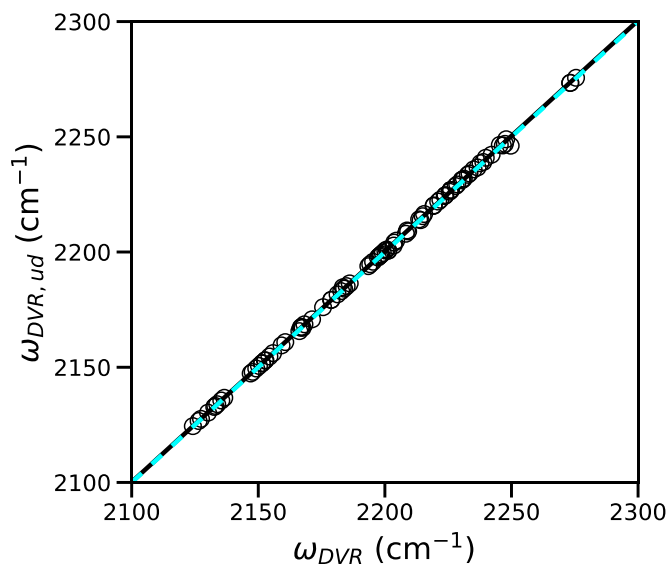

Figure 9. Comparison of DVR frequencies computed using individual localized displacements for each molecule and electronic structure method (ω_{DVR}) and DVR frequencies computed using the universal localized displacements from propyne at MP2/aug-cc-pVTZ, our so called "universal displacements" ($\omega_{DVR,ud}$). The solid black line is a linear fit to the data with the equation $\omega_{DVR,ud} = 1.001\omega_{DVR} - 2.834\ cm^{-1}$. The dotted blue line is $y = x$ for reference. The correlation coefficient for the fit is R = 1.000.

Section 4. The Terminal Alkyne C≡C stretch Vibration

A number of fortunate occurrences allow us to substantially simplify the calculation of terminal alkyne C≡C stretch vibrations. First, the vibration is *localized* to only three atoms for a surprisingly diverse range of molecules, including those that exhibit pi-conjugation. Even in cases where the localization error is larger, the value is still extremely small (60-80 cm^{-1}) compared to

the overall vibrational frequency. Second, the vibration is also anharmonically *isolated*, regardless of the other properties of the molecule. Third, what little error exists between localization and isolation cancels, resulting in a localized DVR method with accuracy comparable to much more expensive methods like VPT2. Fourth, the accuracy carries over to DFT where especially cheap functionals perform extremely well. However, all of our tested DFT functionals show great performance.

These fortunate occurrences allow us to use a relatively cheap DVR method where the same localized normal mode displacements are used for any molecule. This DVR method can be used to calculate vibrational properties like the transition dipole moment and isotropic transition polarizability and our results that broadly match what has been seen in experiment and other theoretical work. Specifically, molecules exhibiting pi-conjugation have especially strong isotropic transition polarizabilities. Meanwhile, molecules with non-carbon atoms directly attached to the alkyne, likely exhibiting strong sigma induction, have strong transition dipole moments.

V. Conclusion

Understanding the terminal alkyne CC stretch vibration is important for a number of biological and materials questions. In this work, we develop and test an extension to the DVR method specific to this important molecular probe. Our resulting localized normal mode DVR method benefits from error cancellation between modest localization and isolation errors. It can be easily implemented using DFT methods and surprisingly TPSS-D3 is a particularly accurate functional when used with it. Finally, we are able to compute important vibrational properties such as the isotropic transition polarizability which are vital for eventually computing Raman spectra in realistic simulations. This method provides a launchpad for the development of a vibrational spectroscopic map for these terminal alkyne vibrational probes and for further investigation of the effects of pi-conjugation and sigma induction on the vibration.

VI. Supplementary Material

Included in the main PDF of our supplementary material are a graph of the comparison between our VPT2 and TOSH frequencies and a table comparing partial and full Hessian localization methods. XYZ files of the investigated molecules optimized with CCSD(T) or MP2 and triple zeta basis sets are also included, because of the large computational cost of obtaining these structures. Finally, JSON data files and instructions for interacting with them in python are included. These JSON files contain all frequencies and localized normal mode CCH displacements computed in this work.

VII. Acknowledgments

VIII. Author Declarations

The authors have no conflicts to disclose. **Kristina Streu**: formal analysis, investigation, methodology, software, supervision, validation, visualization, original draft preparation, review and editing. **Sara Hunsberger**: formal analysis, methodology, investigation, software, review and editing. **Jeanette Patel**: investigation, software, visualization, review and editing. **Xiang Wan**: formal analysis, methodology. **Clyde A. Daly Jr.**: conceptualization, formal analysis, funding acquisition, investigation, methodology, administration, resources, software, supervision, validation, visualization, original draft preparation, review and editing.

IX. Data Availability Statement

The vibrational frequencies and localized normal mode CCH displacements calculated in this work are available as supporting materials, as are CCSD(T) and MP2 structures of the investigated molecules. The general methods and code used to complete the calculations are or soon will be available on github at https://github.com/Daly-Lab-at-Haverford/code_examples. Other data supporting the findings of this study are available upon reasonable request.

X. References

[1] C.R. Baiz, B. Błasiak, J. Bredenbeck, M. Cho, J.-H. Choi, S.A. Corcelli, A.G. Dijkstra, C.-J. Feng, S. Garrett-Roe, N.-H. Ge, M.W.D. Hanson-Heine, J.D. Hirst, T.L.C. Jansen, K. Kwac, K.J. Kubarych, C.H. Londergan, H. Maekawa, M. Reppert, S. Saito, S. Roy, J.L. Skinner, G. Stock, J.E. Straub, M.C. Thielges, K. Tominaga, A. Tokmakoff, H. Torii, L. Wang, L.J. Webb, and M.T. Zanni, "Vibrational Spectroscopic Map, Vibrational Spectroscopy, and Intermolecular Interaction," Chem. Rev. **120**(15), 7152–7218 (2020).

[2] A. Ghosh, J.S. Ostrander, and M.T. Zanni, "Watching Proteins Wiggle: Mapping Structures with Two-Dimensional Infrared Spectroscopy," Chem. Rev. **117**(16), 10726–10759 (2017).

[3] V. Mazzacurati, M.A. Ricci, G. Ruocco, and M. Sampoli, "Low-frequency Raman spectra of liquid water: A molecular dynamics simulation," Chem. Phys. Lett. **159**(4), 383–387 (1989).

[4] M. R. Fagiani, H. Knorke, T. K. Esser, N. Heine, C. T. Wolke, S. Gewinner, W. Schöllkopf, M.-P. Gaigeot, R. Spezia, M. A. Johnson, and K. R. Asmis, "Gas phase vibrational spectroscopy of the protonated water pentamer: the role of isomers and nuclear quantum effects," Phys. Chem. Chem. Phys. **18**(38), 26743–26754 (2016).

[5] K. E. Otto, Z. Xue, P. Zielke, and M. A. Suhm, "The Raman spectrum of isolated water clusters," Phys. Chem. Chem. Phys. **16**(21), 9849–9858 (2014).

[6] S.H. Melfi, J.D. Lawrence Jr., and M.P. McCormick, "OBSERVATION OF RAMAN SCATTERING BY WATER VAPOR IN THE ATMOSPHERE," Appl. Phys. Lett. **15**(9), 295–297 (2003).

[7] K. Dahl, G.M. Sando, D.M. Fox, T.E. Sutto, and J.C. Owrutsky, "Vibrational spectroscopy and dynamics of small anions in ionic liquid solutions," J. Chem. Phys. **123**(8), 084504 (2005).

[8] H.R. Wyss, and M. Falk, "Infrared spectrum of HDO in water and in NaCl solution," Can. J. Chem. **48**(4), 607–614 (1970).

[9] A. Rohman, A. Windarsih, E. Lukitaningsih, M. Rafi, K. Betania, and N.A. Fadzillah, "The use of FTIR and Raman spectroscopy in combination with chemometrics for analysis of biomolecules in biomedical fluids: A review," Biomed. Spectrosc. Imaging **8**(3–4), 55–71 (2019).

[10] A. Orlando, F. Franceschini, C. Muscas, S. Pidkova, M. Bartoli, M. Rovere, and A. Tagliaferro, "A Comprehensive Review on Raman Spectroscopy Applications," Chemosensors **9**(9), 262 (2021).

[11] D.J. Floisand, T.C. Miller, and S.A. Corcelli, "Dynamics and Vibrational Spectroscopy of Alcohols in Ionic Liquids: Methanol and Ethanol," J. Phys. Chem. B **123**(38), 8113–8122 (2019).

[12] S.A. Corcelli, and J.L. Skinner, "Infrared and Raman Line Shapes of Dilute HOD in Liquid H_2O and D_2O from 10 to 90 °C," J. Phys. Chem. A **109**(28), 6154–6165 (2005).

[13] O.O. Mesele, and W.H. Thompson, "A 'Universal' Spectroscopic Map for the OH Stretching Mode in Alcohols," J. Phys. Chem. A **121**(31), 5823–5833 (2017).

[14] B.A. Lindquist, and S.A. Corcelli, "Nitrile Groups as Vibrational Probes: Calculations of the C≡N Infrared Absorption Line Shape of Acetonitrile in Water and Tetrahydrofuran," J. Phys. Chem. B **112**(20), 6301–6303 (2008).

[15] C.M. Morales, and W.H. Thompson, "Simulations of Infrared Spectra of Nanoconfined Liquids: Acetonitrile Confined in Nanoscale, Hydrophilic Silica Pores," J. Phys. Chem. A **113**(10), 1922–1933 (2009).

[16] S.C. Edington, J.C. Flanagan, and C.R. Baiz, "An Empirical IR Frequency Map for Ester C=O Stretching Vibrations," J. Phys. Chem. A **120**(22), 3888–3896 (2016).

[17] S.H. Schneider, and S.G. Boxer, "Vibrational Stark Effects of Carbonyl Probes Applied to Reinterpret IR and Raman Data for Enzyme Inhibitors in Terms of Electric Fields at the Active Site," J. Phys. Chem. B **120**(36), 9672–9684 (2016).

[18] C.I. Drexler, O.M. Cracchiolo, R.L. Myers, H.I. Okur, A.L. Serrano, S.A. Corcelli, and P.S. Cremer, "Local Electric Fields in Aqueous Electrolytes," J. Phys. Chem. B **125**(30), 8484–8493 (2021).

[19] M.W. Lee, J.K. Carr, M. Göllner, P. Hamm, and M. Meuwly, "2D IR spectra of cyanide in water investigated by molecular dynamics simulations," J. Chem. Phys. **139**(5), 054506 (2013).

[20] S.A. Yamada, W.H. Thompson, and M.D. Fayer, "Water-anion hydrogen bonding dynamics: Ultrafast IR experiments and simulations," J. Chem. Phys. **146**(23), 234501 (2017).

[21] J.K. Carr, L.E. Buchanan, J.R. Schmidt, M.T. Zanni, and J.L. Skinner, "Structure and Dynamics of Urea/Water Mixtures Investigated by Vibrational Spectroscopy and Molecular Dynamics Simulation," J. Phys. Chem. B **117**(42), 13291–13300 (2013).

[22] S.M. Gruenbaum, C.J. Tainter, L. Shi, Y. Ni, and J.L. Skinner, "Robustness of Frequency, Transition Dipole, and Coupling Maps for Water Vibrational Spectroscopy," J. Chem. Theory Comput. **9**(7), 3109–3117 (2013).

[23] C.A. Daly, T. Brinzer, C. Allison, S. Garrett-Roe, and S.A. Corcelli, "Enthalpic Driving Force for the Selective Absorption of CO_2 by an Ionic Liquid," J. Phys. Chem. Lett. **9**(6), 1393–1397 (2018).

[24] T. Brinzer, E.J. Berquist, Z.(任哲) Ren, S. Dutta, C.A. Johnson, C.S. Krisher, D.S. Lambrecht, and S. Garrett-Roe, "Ultrafast vibrational spectroscopy (2D-IR) of CO_2 in ionic liquids: Carbon capture from carbon dioxide's point of view," J. Chem. Phys. **142**(21), 212425 (2015).

[25] T. Brinzer, C.A.Jr. Daly, C. Allison, S. Garrett-Roe, and S.A. Corcelli, "Modeling Carbon Dioxide Vibrational Frequencies in Ionic Liquids: III. Dynamics and Spectroscopy," J. Phys. Chem. B **122**(38), 8931–8942 (2018).

[26] S. Egoshi, K. Dodo, K. Ohgane, and M. Sodeoka, "Deuteration of terminal alkynes realizes simultaneous live cell Raman imaging of similar alkyne-tagged biomolecules," Org. Biomol. Chem. **19**(38), 8232–8236 (2021).

[27] K. Koike, K. Bando, J. Ando, H. Yamakoshi, N. Terayama, K. Dodo, N.I. Smith, M. Sodeoka, and K. Fujita, "Quantitative Drug Dynamics Visualized by Alkyne-Tagged Plasmonic-Enhanced Raman Microscopy," ACS Nano **14**(11), 15032–15041 (2020).

[28] S. Bakthavatsalam, K. Dodo, and M. Sodeoka, "A decade of alkyne-tag Raman imaging (ATRI): applications in biological systems," RSC Chem. Biol. **2**(5), 1415–1429 (2021).

[29] H. Yamakoshi, K. Dodo, A. Palonpon, J. Ando, K. Fujita, S. Kawata, and M. Sodeoka, "Alkyne-Tag Raman Imaging for Visualization of Mobile Small Molecules in Live Cells," J. Am. Chem. Soc. **134**(51), 20681–20689 (2012).

[30] M.L. Patterson, and M.J. Weaver, "Surface-enhanced Raman spectroscopy as a probe of adsorbate-surface bonding: simple alkenes and alkynes adsorbed at gold electrodes," J. Phys. Chem. **89**(23), 5046–5051 (1985).

[31] M. Schütz, C.I. Müller, M. Salehi, C. Lambert, and S. Schlücker, "Design and synthesis of Raman reporter molecules for tissue imaging by immuno-SERS microscopy," J. Biophotonics **4**(6), 453–463 (2011).

[32] L. Shi, L. Zhang, and Y. Tian, "Rational Design of Surface-Enhanced Raman Scattering Substrate for Highly Reproducible Analysis," Anal. Sens. **3**(2), e202200064 (2023).

[33] A.L. Malinovsky, A.A. Makarov, and E.A. Ryabov, "Intramolecular vibrational dynamics of propyne and its derivatives: The role of vibrational-rotational mixing," J. Exp. Theor. Phys. **106**(1), 34–45 (2008).

[34] V.F. Kalasinsky, and T.S. Little, "Raman spectra and vibrational dephasing of methylacetylene," J. Raman Spectrosc. **14**(4), 253–258 (1983).

[35] Y. Shen, F. Hu, and W. Min, "Raman Imaging of Small Biomolecules," Annu. Rev. Biophys. **48**(1), 347–369 (2019).

[36] L.T. Wilson, W.J. Tipping, L.E. Jamieson, C. Wetherill, Z. Henley, K. Faulds, D. Graham, S.P. Mackay, and N.C.O. Tomkinson, "A new class of ratiometric small molecule intracellular pH sensors for Raman microscopy," Analyst **145**(15), 5289–5298 (2020).

[37] J.D. Flynn, M.Y. Gimmen, D.N. Dean, S.M. Lacy, and J.C. Lee, "Terminal Alkynes as Raman Probes of α-Synuclein in Solution and in Cells," ChemBioChem **21**(11), 1582–1586 (2020).

[38] M.G. Romei, E.V. von Krusenstiern, S.T. Ridings, R.N. King, J.C. Fortier, C.A. McKeon, K.M. Nichols, L.K. Charkoudian, and C.H. Londergan, "Frequency Changes in Terminal Alkynes Provide Strong, Sensitive, and Solvatochromic Raman Probes of Biochemical Environments," J. Phys. Chem. B **127**(1), 85–94 (2023).

[39] S.C. Epstein, A.R. Huff, E.S. Winesett, C.H. Londergan, and L.K. Charkoudian, "Tracking carrier protein motions with Raman spectroscopy," Nat. Commun. **10**(1), 2227 (2019).

[40] K. Dodo, K. Fujita, and M. Sodeoka, "Raman Spectroscopy for Chemical Biology Research," J. Am. Chem. Soc. **144**(43), 19651–19667 (2022).

[41] X. Bi, K. Miao, and L. Wei, "Alkyne-Tagged Raman Probes for Local Environmental Sensing by Hydrogen–Deuterium Exchange," J. Am. Chem. Soc. **144**(19), 8504–8514 (2022).

[42] T. Dong, P. Yu, J. Zhao, and J. Wang, "Probing the local structure and dynamics of nucleotides using vibrationally enhanced alkynyl stretching," Phys. Chem. Chem. Phys. **24**(48), 29988–29998 (2022).

[43] Y. Li, K.M. Townsend, R.S. Dorn, J.A. Prescher, and E.O. Potma, "Enhancing Alkyne-Based Raman Tags with a Sulfur Linker," J. Phys. Chem. B **127**(9), 1976–1982 (2023).

44 S. Li, T. Chen, Y. Wang, L. Liu, F. Lv, Z. Li, Y. Huang, K.S. Schanze, and S. Wang, "Conjugated Polymer with Intrinsic Alkyne Units for Synergistically Enhanced Raman Imaging in Living Cells," Angew. Chem. Int. Ed. **56**(43), 13455–13458 (2017).

45 S. Tian, H. Li, Z. Li, H. Tang, M. Yin, Y. Chen, S. Wang, Y. Gao, X. Yang, F. Meng, J.W. Lauher, P. Wang, and L. Luo, "Polydiacetylene-based ultrastrong bioorthogonal Raman probes for targeted live-cell Raman imaging," Nat. Commun. **11**(1), 81 (2020).

46 D. Kossowska, G. Lee, H. Han, K. Kwak, and M. Cho, "Simultaneous enhancement of transition dipole strength and vibrational lifetime of an alkyne IR probe via π-d backbonding and vibrational decoupling," Phys. Chem. Chem. Phys. **21**(45), 24919–24925 (2019).

47 D. Kossowska, K. Park, J.Y. Park, C. Lim, K. Kwak, and M. Cho, "Rational Design of an Acetylenic Infrared Probe with Enhanced Dipole Strength and Increased Vibrational Lifetime," J. Phys. Chem. B **123**(29), 6274–6281 (2019).

48 E.B. Wilson, *Molecular Vibrations: The Theory of Infrared and Raman Vibrational Spectra* (Courier Dover Publications, 1955).

49 J. Stare, "First-Principle Calculation of Reduced Masses in Vibrational Analysis Using Generalized Internal Coordinates: Some Crucial Aspects and Examples," J. Chem. Inf. Model. **47**(3), 840–850 (2007).

50 D. McQuarrie, *Quantum Chemistry*, 2nd ed. (University Science Books, Sausalito, California, 2008).

51 C.Y. Lin, A.T.B. Gilbert, and P.M.W. Gill, "Calculating molecular vibrational spectra beyond the harmonic approximation," Theor. Chem. Acc. **120**(1), 23–35 (2008).

52 R.J. Whitehead, and N.C. Handy, "Variational calculation of vibration-rotation energy levels for triatomic molecules," J. Mol. Spectrosc. **55**(1), 356–373 (1975).

53 A. Adel, and D.M. Dennison, "The Infrared Spectrum of Carbon Dioxide. Part I," Phys. Rev. **43**(9), 716–723 (1933).

54 J.M. Bowman, "Self-consistent field energies and wavefunctions for coupled oscillators," J. Chem. Phys. **68**(2), 608–610 (2008).

55 D.T. Colbert, and W.H. Miller, "A novel discrete variable representation for quantum mechanical reactive scattering via the S-matrix Kohn method," J. Chem. Phys. **96**(3), 1982–1991 (1992).

56 C. Schwartz, "High-accuracy approximation techniques for analytic functions," J. Math. Phys. **26**(3), 411–415 (1985).

57 J.C. Light, and T. Carrington Jr., in *Adv. Chem. Phys.* (John Wiley & Sons, Ltd, 2000), pp. 263–310.

58 G.C. Groenenboom, and D.T. Colbert, "Combining the discrete variable representation with the S-matrix Kohn method for quantum reactive scattering," J. Chem. Phys. **99**(12), 9681 (1998).

59 N.M. Levinson, E.E. Bolte, C.S. Miller, S.A. Corcelli, and S.G. Boxer, "Phosphate Vibrations Probe Local Electric Fields and Hydration in Biomolecules," J. Am. Chem. Soc. **133**(34), 13236–13239 (2011).

60 C.A. Daly, L.M. Streacker, Y. Sun, S.R. Pattenaude, A.A. Hassanali, P.B. Petersen, S.A. Corcelli, and D. Ben-Amotz, "Decomposition of the Experimental Raman and Infrared Spectra of Acidic Water into Proton, Special Pair, and Counterion Contributions," J. Phys. Chem. Lett. **8**(21), 5246–5252 (2017).

61 E.J. Berquist, C.A. Daly, T. Brinzer, K.K. Bullard, Z.M. Campbell, S.A. Corcelli, S. Garrett-Roe, and D.S. Lambrecht, "Modeling Carbon Dioxide Vibrational Frequencies in Ionic Liquids: I. Ab Initio Calculations," J. Phys. Chem. B **121**(1), 208–220 (2017).

62 S.K. Gray, and G.G. Balint-Kurti, "Quantum dynamics with real wave packets, including application to three-dimensional (J=0)D+H2→HD+H reactive scattering," J. Chem. Phys. **108**(3), 950–962 (1998).

[63] N. He, M. Huang, and F.A. Evangelista, "CO Inversion on a NaCl(100) Surface: A Multireference Quantum Embedding Study," J. Phys. Chem. A **127**(8), 1975–1987 (2023).

[64] K. Blöndal, K. Sargsyan, D.H. Bross, B. Ruscic, and C.F. Goldsmith, "Configuration Space Integration for Adsorbate Partition Functions: The Effect of Anharmonicity on the Thermophysical Properties of CO–Pt(111) and CH3OH–Cu(111)," ACS Catal. **13**(1), 19–32 (2023).

[65] J. Neugebauer, M. Reiher, C. Kind, and B.A. Hess, "Quantum chemical calculation of vibrational spectra of large molecules—Raman and IR spectra for Buckminsterfullerene," J. Comput. Chem. **23**(9), 895–910 (2002).

[66] D.A. McQuarrie, *Statistical Mechanics* (Harper & Row, 1975).

[67] P. Vandenabeele, and D.J. Ando, *Practical Raman Spectroscopy: An Introduction* (John Wiley & Sons, Incorporated, Hoboken, 2013).

[68] J.C. Slater, "A Simplification of the Hartree-Fock Method," Phys. Rev. **81**(3), 385–390 (1951).

[69] Chr. Møller, and M.S. Plesset, "Note on an Approximation Treatment for Many-Electron Systems," Phys. Rev. **46**(7), 618–622 (1934).

[70] K. Raghavachari, G.W. Trucks, J.A. Pople, and M. Head-Gordon, "A fifth-order perturbation comparison of electron correlation theories," Chem. Phys. Lett. **157**(6), 479–483 (1989).

[71] A.D. Becke, "Density-functional thermochemistry. III. The role of exact exchange," J. Chem. Phys. **98**(7), 5648–5652 (1993).

[72] C. Lee, W. Yang, and R.G. Parr, "Development of the Colle-Salvetti correlation-energy formula into a functional of the electron density," Phys. Rev. B **37**(2), 785–789 (1988).

[73] P.J. Stephens, F.J. Devlin, C.F. Chabalowski, and M.J. Frisch, "Ab Initio Calculation of Vibrational Absorption and Circular Dichroism Spectra Using Density Functional Force Fields," J. Phys. Chem. **98**(45), 11623–11627 (1994).

[74] S. Grimme, S. Ehrlich, and L. Goerigk, "Effect of the damping function in dispersion corrected density functional theory," J. Comput. Chem. **32**(7), 1456–1465 (2011).

[75] N. Mardirossian, and M. Head-Gordon, "ωB97M-V: A combinatorially optimized, range-separated hybrid, meta-GGA density functional with VV10 nonlocal correlation," J. Chem. Phys. **144**(21), 214110 (2016).

[76] J. Tao, J.P. Perdew, V.N. Staroverov, and G.E. Scuseria, "Climbing the Density Functional Ladder: Nonempirical Meta–Generalized Gradient Approximation Designed for Molecules and Solids," Phys. Rev. Lett. **91**(14), 146401 (2003).

[77] S. Grimme, J.G. Brandenburg, C. Bannwarth, and A. Hansen, "Consistent structures and interactions by density functional theory with small atomic orbital basis sets," J. Chem. Phys. **143**(5), 054107 (2015).

[78] E. Epifanovsky, A.T.B. Gilbert, X. Feng, J. Lee, Y. Mao, N. Mardirossian, P. Pokhilko, A.F. White, M.P. Coons, A.L. Dempwolff, Z. Gan, D. Hait, P.R. Horn, L.D. Jacobson, I. Kaliman, J. Kussmann, A.W. Lange, K.U. Lao, D.S. Levine, J. Liu, S.C. McKenzie, A.F. Morrison, K.D. Nanda, F. Plasser, D.R. Rehn, M.L. Vidal, Z.-Q. You, Y. Zhu, B. Alam, B.J. Albrecht, A. Aldossary, E. Alguire, J.H. Andersen, V. Athavale, D. Barton, K. Begam, A. Behn, N. Bellonzi, Y.A. Bernard, E.J. Berquist, H.G.A. Burton, A. Carreras, K. Carter-Fenk, R. Chakraborty, A.D. Chien, K.D. Closser, V. Cofer-Shabica, S. Dasgupta, M. de Wergifosse, J. Deng, M. Diedenhofen, H. Do, S. Ehlert, P.-T. Fang, S. Fatehi, Q. Feng, T. Friedhoff, J. Gayvert, Q. Ge, G. Gidofalvi, M. Goldey, J. Gomes, C.E. González-Espinoza, S. Gulania, A.O. Gunina, M.W.D. Hanson-Heine, P.H.P. Harbach, A. Hauser, M.F. Herbst, M. Hernández Vera, M. Hodecker, Z.C. Holden, S. Houck, X. Huang, K. Hui, B.C. Huynh, M. Ivanov, Á. Jász, H. Ji, H. Jiang, B. Kaduk, S. Kähler, K. Khistyaev, J. Kim, G. Kis, P. Klunzinger, Z. Koczor-Benda, J.H. Koh, D. Kosenkov, L. Koulias, T. Kowalczyk, C.M. Krauter, K. Kue, A. Kunitsa, T. Kus, I. Ladjánszki, A. Landau, K.V. Lawler, D. Lefrancois, S. Lehtola, R.R. Li, Y.-P. Li, J. Liang, M. Liebenthal, H.-H. Lin, Y.-S. Lin, F. Liu, K.-Y. Liu, M. Loipersberger, A. Luenser, A. Manjanath, P. Manohar, E. Mansoor, S.F. Manzer, S.-P. Mao, A.V. Marenich, T. Markovich, S. Mason, S.A. Maurer, P.F.

McLaughlin, M.F.S.J. Menger, J.-M. Mewes, S.A. Mewes, P. Morgante, J.W. Mullinax, K.J. Oosterbaan, G. Paran, A.C. Paul, S.K. Paul, F. Pavošević, Z. Pei, S. Prager, E.I. Proynov, Á. Rák, E. Ramos-Cordoba, B. Rana, A.E. Rask, A. Rettig, R.M. Richard, F. Rob, E. Rossomme, T. Scheele, M. Scheurer, M. Schneider, N. Sergueev, S.M. Sharada, W. Skomorowski, D.W. Small, C.J. Stein, Y.-C. Su, E.J. Sundstrom, Z. Tao, J. Thirman, G.J. Tornai, T. Tsuchimochi, N.M. Tubman, S.P. Veccham, O. Vydrov, J. Wenzel, J. Witte, A. Yamada, K. Yao, S. Yeganeh, S.R. Yost, A. Zech, I.Y. Zhang, X. Zhang, Y. Zhang, D. Zuev, A. Aspuru-Guzik, A.T. Bell, N.A. Besley, K.B. Bravaya, B.R. Brooks, D. Casanova, J.-D. Chai, S. Coriani, C.J. Cramer, G. Cserey, A.E. DePrince III, R.A. DiStasio Jr., A. Dreuw, B.D. Dunietz, T.R. Furlani, W.A. Goddard III, S. Hammes-Schiffer, T. Head-Gordon, W.J. Hehre, C.-P. Hsu, T.-C. Jagau, Y. Jung, A. Klamt, J. Kong, D.S. Lambrecht, W. Liang, N.J. Mayhall, C.W. McCurdy, J.B. Neaton, C. Ochsenfeld, J.A. Parkhill, R. Peverati, V.A. Rassolov, Y. Shao, L.V. Slipchenko, T. Stauch, R.P. Steele, J.E. Subotnik, A.J.W. Thom, A. Tkatchenko, D.G. Truhlar, T. Van Voorhis, T.A. Wesolowski, K.B. Whaley, H.L. Woodcock III, P.M. Zimmerman, S. Faraji, P.M.W. Gill, M. Head-Gordon, J.M. Herbert, and A.I. Krylov, "Software for the frontiers of quantum chemistry: An overview of developments in the Q-Chem 5 package," J. Chem. Phys. **155**(8), 084801 (2021).

[79] M. Bursch, J.-M. Mewes, A. Hansen, and S. Grimme, "Best-Practice DFT Protocols for Basic Molecular Computational Chemistry**," Angew. Chem. Int. Ed. **61**(42), e202205735 (2022).

[80] P. Morgante, and R. Peverati, "The devil in the details: A tutorial review on some undervalued aspects of density functional theory calculations," Int. J. Quantum Chem. **120**(18), e26332 (2020).

[81] A. Schäfer, H. Horn, and R. Ahlrichs, "Fully optimized contracted Gaussian basis sets for atoms Li to Kr," J. Chem. Phys. **97**(4), 2571–2577 (1992).

[82] T.H. Dunning Jr., "Gaussian basis sets for use in correlated molecular calculations. I. The atoms boron through neon and hydrogen," J. Chem. Phys. **90**(2), 1007–1023 (1989).

[83] J.S. Binkley, J.A. Pople, and W.J. Hehre, "Self-consistent molecular orbital methods. 21. Small split-valence basis sets for first-row elements," J. Am. Chem. Soc. **102**(3), 939–947 (1980).

[84] P. Pulay, "Improved SCF convergence acceleration," J. Comput. Chem. **3**(4), 556–560 (1982).

[85] E. Cancès, and C. Le Bris, "Can we outperform the DIIS approach for electronic structure calculations?," Int. J. Quantum Chem. **79**(2), 82–90 (2000).

[86] S.-H. Chien, and P.M.W. Gill, "SG-0: A small standard grid for DFT quadrature on large systems," J. Comput. Chem. **27**(6), 730–739 (2006).

[87] A.G. Gale, T.T. Odbadrakh, B.T. Ball, and G.C. Shields, "Water-Mediated Peptide Bond Formation in the Gas Phase: A Model Prebiotic Reaction," J. Phys. Chem. A **124**(20), 4150–4159 (2020).

[88] S. Xu, J.M. Nilles, and K.H. Bowen Jr., "Zwitterion formation in hydrated amino acid, dipole bound anions: How many water molecules are required?," J. Chem. Phys. **119**(20), 10696–10701 (2003).

[89] P.T. Panek, and C.R. Jacob, "Efficient Calculation of Anharmonic Vibrational Spectra of Large Molecules with Localized Modes," ChemPhysChem **15**(15), 3365–3377 (2014).

[90] X. Cheng, and R.P. Steele, "Efficient anharmonic vibrational spectroscopy for large molecules using local-mode coordinates," J. Chem. Phys. **141**(10), 104105 (2014).

[91] A. Ghysels, D. Van Neck, V. Van Speybroeck, T. Verstraelen, and M. Waroquier, "Vibrational modes in partially optimized molecular systems," J. Chem. Phys. **126**(22), 224102 (2007).

[92] C.R. Jacob, and M. Reiher, "Localizing normal modes in large molecules," J. Chem. Phys. **130**(8), 084106 (2009).

[93] E. Kraka, W. Zou, and Y. Tao, "Decoding chemical information from vibrational spectroscopy data: Local vibrational mode theory," WIREs Comput. Mol. Sci. **10**(5), e1480 (2020).

94 E. Kraka, M. Quintano, H.W. La Force, J.J. Antonio, and M. Freindorf, "The Local Vibrational Mode Theory and Its Place in the Vibrational Spectroscopy Arena," J. Phys. Chem. A **126**(47), 8781–8798 (2022).

95 N.A. Besley, and J.A. Bryan, "Partial Hessian Vibrational Analysis of Organic Molecules Adsorbed on Si(100)," J. Phys. Chem. C **112**(11), 4308–4314 (2008).

96 N.A. Besley, and K.A. Metcalf, "Computation of the amide I band of polypeptides and proteins using a partial Hessian approach," J. Chem. Phys. **126**(3), (2007).

97 P. Linstrom, "NIST Chemistry WebBook, NIST Standard Reference Database 69," (1997).

98 R. Johnson, "Computational Chemistry Comparison and Benchmark Database, NIST Standard Reference Database 101," (2002).

99 O. Bastiansen, P. Bakken, E. Kloster-Jensen, S. Samdal, and M. Trætteberg, "A theoretical and experimental study of the molecular structure of 1-butyne," J. Mol. Struct. **352–353**, 77–85 (1995).

100 G.W. King, and D. Moule, "I&a-red and Raman spectra of propynal," (n.d.).

101 R. Hochstrasser, and J. Wirz, "Ethinol: Photochemische Erzeugung in einer Argonmatrix, IR-Spektrum und Photoisomerisierung zu Keten," Angew. Chem. **101**(2), 183–185 (1989).

102 Curt. Wentrup, Horst. Briehl, Primoz. Lorencak, U.J. Vogelbacher, H.Wilhelm. Winter, Andre. Maquestiau, and Robert. Flammang, "Primary ethynamines (HC.tplbond.CNH2, PhC.tplbond.CNH2), aminopropadienone (H2NCH:C:C:O), and imidoylketene (HN:CHCH:C:O). Preparation and identification of molecules of cosmochemical interest," J. Am. Chem. Soc. **110**(5), 1337–1343 (1988).

103 T. Shimanouchi, "Tables of molecular vibrational frequencies, consolidated volume I," (n.d.).

104 R.A. Nyquist, "Vibrational assignments of H-CC-CH2OH and its deuterium analogs," Spectrochim. Acta **27A**, 2513–2523 (1971).

105 J.H. Wotiz, F.A. Miller, and R.J. Palchak, "The Infrared Spectra of Propargylic Alcohols and Bromides," ACS Publ., (2002).

106 John Wiley & Sons, Inc. SpectraBase, "Propargyl Alcohol; SpectraBase Compound ID=H6fwKPZI5R2," (n.d.).

107 S. Guan, G.A. Attard, and A.J. Wain, "Observation of Substituent Effects in the Electrochemical Adsorption and Hydrogenation of Alkynes on Pt{hkl} Using SHINERS," ACS Catal. **10**(19), 10999–11010 (2020).

108 F. Jørgensen, "Orientation of the Eckart frame in a polyatomic molecule by symmetric orthonormalization," Int. J. Quantum Chem. **14**(1), 55–63 (1978).

109 K.K. Irikura, R.D. Johnson, and R.N. Kacker, "Uncertainties in Scaling Factors for ab Initio Vibrational Frequencies," J. Phys. Chem. A **109**(37), 8430–8437 (2005).

110 H.D. Downing, B.J. Krohn, and R.H. Hunt, "Coriolis intensity perturbations in Π-Σ bands of CO2," J. Mol. Spectrosc. **55**(1), 66–80 (1975).

111 C.A. Daly, E.J. Berquist, T. Brinzer, S. Garrett-Roe, D.S. Lambrecht, and S.A. Corcelli, "Modeling Carbon Dioxide Vibrational Frequencies in Ionic Liquids: II. Spectroscopic Map," J. Phys. Chem. B **120**(49), 12633–12642 (2016).

112 G. Tejeda, B. Maté, and S. Montero, "Overtone Raman spectrum and molecular polarizability surface of CO2," J. Chem. Phys. **103**(2), 568–576 (1995).